

# Tapless Voltage Regulating Transformer Final Report



Zhi Li  
Bailu Xiao  
Yaosuo Xue  
Philip Irminger

**September 2020**

**Approved for public release.  
Distribution is unlimited.**

## DOCUMENT AVAILABILITY

Reports produced after January 1, 1996, are generally available free via US Department of Energy (DOE) SciTech Connect.

**Website** [www.osti.gov](http://www.osti.gov)

Reports produced before January 1, 1996, may be purchased by members of the public from the following source:

National Technical Information Service  
5285 Port Royal Road  
Springfield, VA 22161  
**Telephone** 703-605-6000 (1-800-553-6847)  
**TDD** 703-487-4639  
**Fax** 703-605-6900  
**E-mail** [info@ntis.gov](mailto:info@ntis.gov)  
**Website** <http://classic.ntis.gov/>

Reports are available to DOE employees, DOE contractors, Energy Technology Data Exchange representatives, and International Nuclear Information System representatives from the following source:

Office of Scientific and Technical Information  
PO Box 62  
Oak Ridge, TN 37831  
**Telephone** 865-576-8401  
**Fax** 865-576-5728  
**E-mail** [reports@osti.gov](mailto:reports@osti.gov)  
**Website** <http://www.osti.gov/contact.html>

This report was prepared as an account of work sponsored by an agency of the United States Government. Neither the United States Government nor any agency thereof, nor any of their employees, makes any warranty, express or implied, or assumes any legal liability or responsibility for the accuracy, completeness, or usefulness of any information, apparatus, product, or process disclosed, or represents that its use would not infringe privately owned rights. Reference herein to any specific commercial product, process, or service by trade name, trademark, manufacturer, or otherwise, does not necessarily constitute or imply its endorsement, recommendation, or favoring by the United States Government or any agency thereof. The views and opinions of authors expressed herein do not necessarily state or reflect those of the United States Government or any agency thereof.

Electrical and Electronics Systems Research Division

**TAPLESS VOLTAGE REGULATING TRANSFORMER  
FINAL REPORT**

Zhi Li  
Bailu Xiao  
Yaosuo Xue  
Philip Irminger

September 2020

Prepared by  
OAK RIDGE NATIONAL LABORATORY  
Oak Ridge, TN 37831-6283  
managed by  
UT-BATTELLE, LLC  
for the  
US DEPARTMENT OF ENERGY  
under contract DE-AC05-00OR22725



## CONTENTS

|   |     |
|---|-----|
| LIST OF FIGURES .....   | v   |
| LIST OF TABLES .....  | vi  |
| EXECUTIVE SUMMARY .....   | vii |
| 1. OVERVIEW .....   | 1   |
| 1.1 INTRODUCTION .....  | 1   |
| 1.2 GENERAL FINDINGS .....  | 3   |
| 1.3 RELEVANCE AND EFFECTS.....                                      | 4   |
| 2. PROTOTYPES AND TESTING SETUP.....                                | 5   |
| 2.1 BENCHTOP PROTOTYPES .....                                       | 5   |
| 2.2 TESTING AND PRELIMINARY RESULTS.....                            | 6   |
| 3. ANALYSIS MODELS OF TAREX.....                                    | 10  |
| 3.1 OVERVIEW .....  | 10  |
| 3.2 AN ANALYTICAL MODEL OF THE TAREX.....                           | 11  |
| 3.3 FEA MODEL.....  | 16  |
| 3.4 PLECS MODEL .....   | 19  |
| 4. MODEL IMPROVEMENTS AND VALIDATIONS .....                         | 22  |
| 4.1 IMPROVEMENTS BASED ON TESTING.....                              | 22  |
| 4.2 INTEGRATION OF DC CONTROL MODEL.....                            | 24  |
| 4.3 MODELING LEAKAGE INDUCTANCE.....                                | 28  |
| 5. HARMONICS ANALYSIS.....  | 35  |
| 6. CONCLUSIONS .....  | 39  |
| REFERENCES .....  | 41  |
| APPENDIX A. PROTOTYPE PARAMETERS .....                              | A-1 |
| APPENDIX B. FEA MODEL SETUP .....                                   | B-1 |
| APPENDIX C. NETL TESTING REPORT .....                               | C-1 |
| APPENDIX D. DERIVATION OF THE TIME-DOMAIN MODEL OF A DC SOURCE..... | D-1 |



## LIST OF FIGURES

|  |    |
|--|----|
| Figure 1.1. Configuration of a TAREX. ....   | 2  |
| Figure 2.1. The first prototype was retrofitted from a 115:10/20/40 V, 50 VA TRIAD transformer. ....   | 5  |
| Figure 2.2. The second prototype was retrofitted from a 115:115 V, 500 VA TRIAD transformer. ....  | 6  |
| Figure 2.3. Diagram of testing for TAREX prototypes. ....  | 7  |
| Figure 2.4. Test setup and DC power supplies. ....   | 7  |
| Figure 2.5. Results of an open-circuit test on Prototype 1 to show voltage regulation enabled<br>by DC bias control. ....  | 9  |
| Figure 3.1. The equivalent circuit model of a transformer. ....  | 10 |
| Figure 3.1. An MEC model of the three-limb-core transformer shown in Figure 1.1. ....  | 11 |
| Figure 3.2. Magnetic fluxes in the core of TAREX. ....   | 12 |
| Figure 3.3. One MEC model for TAREX with the MMF sources of DC. ....   | 12 |
| Figure 3.4. Flow chart of the MATLAB program to implement the analytical model of the<br>TAREX. ....   | 14 |
| Figure 3.5. (top) Winding currents of the three windings and (bottom) the B fields in the<br>three core limbs calculated using the TAREX analytical model. ....                      | 15 |
| Figure 3.6. Results comparisons between the analytical model, Plecs model, and testing (for<br>prototype 1 with load resistance = 15 $\Omega$ ). ....                                | 16 |
| Figure 3.7. The 3D FEA model of Prototype 2, showing the leakage channel defined<br>to calculate the winding leakages. ....  | 17 |
| Figure 3.8. Applying AC voltage source in the primary winding with or without ramping, and the<br>corresponding induced currents in the same winding. ....                           | 19 |
| Figure 3.9. A Plecs model of the TAREX. ....   | 20 |
| Figure 4.1. B-H curve of M19 steel and the measured B-H curve of the core steel of Prototype 2. ....   | 23 |
| Figure 4.2. Improvement by using the new B-H curve of the core measured by the NETL team<br>(test on Prototype 2, loading resistor = 56 $\Omega$ ). ....                             | 24 |
| Figure 4.3. Results of the winding voltage, updated model (using voltage source model)<br>vs. the previous model (NETL curve in Figure 4.2). ....                                    | 25 |
| Figure 4.4. Induced voltage on DC winding and ripples in DC current supply,<br>(a) calculations vs. (b) measurements. ....   | 26 |
| Figure 4.5. The equivalent circuit and frequency domain model of a DCC. ....   | 27 |
| Figure 4.6. (a) Test setup and (b) waveforms snapshot of the leakage measurement test (by the<br>NETL team). ....  | 28 |
| Figure 4.7. The effect of DC bias on the leakage inductance. ....  | 31 |
| Figure 4.1. Effect of winding gap on leakage inductance (by simulated open-circuit<br>test on Prototype 2, DC = 0 A). ....   | 32 |
| Figure 4.2. Calculated leakage inductance with change of DC bias for different winding gaps<br>(by simulated load test on Prototype 2, with a resistance load of 56 $\Omega$ ). .... | 33 |
| Figure 4.3. Voltage regulation curves for different winding gaps (by FEA simulation results on<br>Prototype 2, with a resistance load of 56 $\Omega$ ). ....                         | 34 |
| Figure 5.1. Secondary voltage waveform and harmonics with/without the discussed mitigation<br>method (imposing 2nd harmonics in dc applied to the transformer). ....                 | 36 |
| Figure 5.2. One design of the control to implement the discussed mitigation method. ....   | 36 |
| Figure 5.3. Harmonics mitigation of a transformer under asymmetrical saturation (DC in primary<br>winding) by using DC compensation in the additional control winding. ....          | 37 |

## LIST OF TABLES

|   |    |
|---|----|
| Table 3.1. Excitation source setups for different tests. .... | 17 |
|---|----|



## EXECUTIVE SUMMARY

### ***Background***

In electric power engineering, voltage regulation is used to change the magnitude of voltages in the power grid to maintain near constant voltage over a wide range of load conditions and service areas. It is a common practice in power grid operation, often realized by regulation measures such as an on-load tap changing (OLTC) power transformer, switching capacitor/inductor, and so on. The conventional voltage regulation methods have faced ever-increasing challenges as the penetration of renewable generations deepens in the grid. The intermittent nature of the renewable sources may result in a sudden rise or drop of power generation, which breaks the generation-load balance and causes frequent voltage rises or drops. In some cases, an order of magnitude higher number of voltage regulation actions could be needed when the variation and intermittence of renewable sources are present.<sup>1,2</sup> A lack of adequate voltage control not only affects the power quality but is detrimental to the system operation with the potential for large economic losses.

Most conventional voltage regulation devices rely on mechanical tap changers to impose the regulation in a stepwise manner. Power transformers equipped with the mechanical tap changers can provide  $\pm 10\% \sim 15\%$  variation around the rated voltage, which is sufficient for most cases. Unfortunately, the mechanical tap changers are not capable of frequent and more flexible operation. They can easily wear out in the challenging situations created by renewables. Solid-state-based tap changing technologies have improved performance. However, they are still insufficient to fully address the challenges in a cost-effective way and cannot be broadly adopted unless low-cost, high-rating power electronics devices are readily available.

### ***Technical approach***

In this project, a novel technology called the “tapless voltage-regulating transformer” (TAREX) was proposed and investigated. It has the potential to excel at addressing the new voltage regulation challenges and replace the conventional regulating transformers. The TAREX is based on the concept of the saturable-core reactor. The voltage of a TAREX can be smoothly and continuously regulated in a reasonable range by using a low-rating power electronics-based controller. It uses control of the transformer core magnetization to regulate the voltage on the windings and thus eliminates the mechanical tap changer.

More specifically, the TAREX has similar configurations as typical power transformers, except that an additional winding on the transformer core is introduced for regulation. Direct current (DC) control signals are applied to the control winding, imposing DC magnetic flux to the iron core and shifting the core magnetization back and forth. The change of the magnetization results in the control of the winding voltage. The DC controller is realized by low rating power electronics-based converter systems and is inexpensive and flexible to control. Smooth and continuous variation of the voltage is thus realized safely because of the electrical separation between the main power side and the control circuits.

---

<sup>1</sup> D. Nguyen, P. Ubiratan, M. Velay, R. Hanna, J. Kleissl, J. Schoene, et al., “Impact Research of High Photovoltaics Penetration Using High Resolution Resource Assessment with Sky Imager and Power System Simulation,” *CSI RD&D3 Subtask 4.3 Final Report*, Nov. 2015.

<sup>2</sup> C. K. Gan, C. Y. Lau, K. A. Baharin, and D. Pudjianto, “Impact of the photovoltaic system variability on transformer tap changer operations in distribution networks,” *CIREN - Open Access Proceedings Journal*, vol. 2017, no. 1, pp. 1818–1821, 2017, doi: 10.1049/oap-cired.2017.0476.

The concept of the TAREX is novel and the technology is at relatively low technology readiness level. This project's goals were to prove the principle of the TAREX, understand the voltage regulation mechanism, and preliminarily understand its effects on the power systems through modeling, prototyping, and testing. In this project, benchtop prototypes of the TAREX were developed for validation and testing purposes. The results of the project provide insights into the physics behind the TAREX technology and can be used to guide future R&D work for scaling up.

### ***General findings***

1. The voltage-regulating effect in a TAREX is the result of two major coupled electromagnetic processes—the shifted magnetic induction and the change of winding leakage inductances—simultaneously occurring under the DC flux-biased core magnetization. The overall effect of the two processes is the reduction of the winding voltage as the DC control increases.
2. The voltage regulation of a TAREX can be well modeled by both analytical and numerical methods. Analytical models based on the magnetic equivalent circuit method with some improvements can provide fairly good representations of the regulation process. Finite element analysis models of TAREX allow more flexibilities in modeling magnetic details and thus give more accurate results.
3. The magnetically regulated voltage was, for the first time, demonstrated on the prototypes developed in the project. However, the voltage variation range obtained on the prototypes was limited (less than 5%). To achieve the desired range, a TAREX must be carefully designed. For example, increasing winding gaps, which results in larger leakage inductances, was found in this project to be effective to expand the voltage regulation range. Other parameters such as the core material and Amp-turns ratio of the alternating current (AC) source and DC bias are also important and need to be considered.
4. The DC bias boosted the nonlinearity in the magnetization of the ferromagnetic core, resulting in an increased harmonics level in the induced voltage. One possible harmonics mitigation method was briefly investigated and found to be effective. The method is to impose designed AC components into the DC control current to counter the induced harmonics contents.

### ***Relevance and effects***

The modeling, prototyping, and testing work conducted in this project has established a clear understanding of the mechanisms of magnetically regulating transformer voltage in TAREX. It has demonstrated, for the first time, the concept of a continuous regulation of transformer voltage by controlling the magnetic field. The findings of the project will be valuable technical preparation for the follow-up R&D efforts that may be seeking scaling up and commercialization. Success of the project boosts the confidence of potential sponsors and reduces the risk for their investments. It also benefits the research on similar or related technologies.

Without the need for mechanical switching, the TAREX is durable and resilient. It also should be more affordable than the expensive high-power rating solid-state devices or tap changers. TAREX opens the door to a whole new R&D area that has great potentials of field application in real power systems since power transformers have been the backbone components of modern power systems, transmission, and distribution. It has the potential to solve the urgent challenges that mechanical OLTC faces and fill the gaps between the conventional OLTC and next-generation technologies (e.g., solid-state transformers). It may enable the development of more flexible power transformers that can be used in a variety of situations that would otherwise require custom-designed transformers.

# 1. OVERVIEW

## 1.1 INTRODUCTION

The conventional voltage regulation methods in the power grid have faced increasing challenges as the penetration of renewable generations deepens. The intermittent nature of the renewable sources and their high-switching frequency power electronic interfaces increase the complexities of grid operation and control, resulting in effects on system voltage down to local levels. A lack of adequate voltage control not only affects the power quality but is detrimental to the system operation with the potential for large economic losses. Many cases show that the existing voltage control measures are overwhelmed and insufficient for addressing the new issues. For example, an order of magnitude increase in voltage regulation actions could be needed when the variation and intermittence of renewable sources are present [1]–[2]. The conventional regulation equipment, which is not designed for very frequent operation, would easily wear out in such situations.

A mechanical on-load tap changing (OLTC) power transformer has been the major voltage regulation measure in the power industry. It regulates the voltage at discrete steps by mechanically switching taps on one of the transformer windings (i.e., adjusting the turn ratio between the primary and secondary windings). With a fixed number of taps provided, a typical  $\pm 10\sim 15\%$  variation can be obtained in a stepwise manner. Although proven effective, mechanical OLTC only provides coarse voltage regulation sequentially. The durability of OLTC can be substantially affected as the need for voltage regulation increases with the deepening renewable generation penetration [3]. Although solid-state-based tap changing technologies have improved the switching performance, they are still insufficient to fully address the challenges in a cost-effective way and cannot be broadly adopted unless low-cost, high-power electronic devices are readily available.

In this project, a novel technology called the “tapless voltage-regulating transformer” (TAREX) was investigated. The TAREX is based on the concept of the saturable-core reactor (SCR) [4]–[6] and the continuously variable series reactor, a technology developed by the US Department of Energy’s Oak Ridge National Laboratory [7]–[9]. The voltage of a TAREX can be smoothly and continuously regulated in a reasonable range by using a low-capacity rating power electronics-based controller. It uses the control of the transformer core magnetization to regulate the voltage on the windings and thus eliminates the mechanical tap changer. The project’s goals were to prove the principle of the TAREX, understand the voltage regulation mechanism, and preliminarily assess its effects on power systems. Benchtop prototypes of the TAREX were developed for validation and testing purposes. The results of this project provide insights into the physics behind the TAREX technology and can be used to guide future R&D work for scaling up.

### *Concept of the TAREX*

The TAREX approach employs proven SCR and power electronics technologies in an innovative way to enable voltage regulation in a transformer. The single-phase TAREX design investigated in the project is shown in Figure 1.1. The same as a typical shell-type transformer, the primary and secondary windings of the transformer are wound on the middle leg of the ferromagnetic core. Two separated coils are wound on the outer legs to form an additional set of winding for voltage regulation control. It is called the direct current (DC) or control winding because a DC controller will be connected to it to impose the DC flux to the transformer core and regulate the voltage. The two coils are connected in a counter-series manner to avoid the large induced voltage from the alternating current (AC) side. The design is magnetically similar to the SCR, with the exception of the number of AC windings (one AC winding for the SCR, whereas two or more windings for the transformer). The DC controller is realized by low-capacity rating power electronic devices. Besides smooth and continuous variation of the voltage on one of the AC windings,

another major advantage of TAREX is the electrical separation between the AC and DC circuits for enhanced reliability.

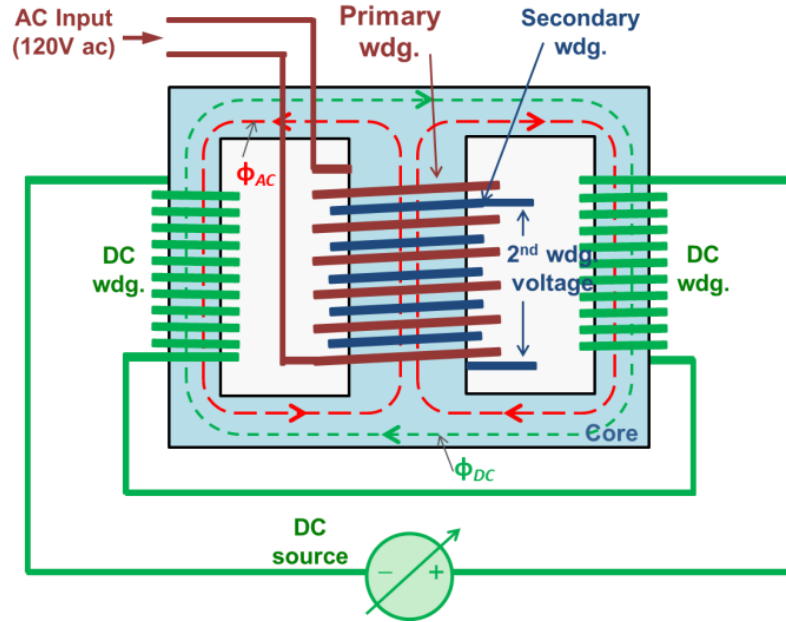


**Figure 1.1. Configuration of a TAREX.**

The operation of a TAREX is equivalent to the conventional transformer, both electrically and magnetically if there is no control current applied. When the control is imposed, DC is present in the control winding, thereby generating DC flux to shift the magnetization of the transformer core. One of the two outer legs will be saturated depending on the direction of the AC magnetizing flux in the transformer. Consequently, the AC reluctance and the leakage flux in the AC windings are changed, and the induced voltage in the AC windings changes accordingly. Given enough DC control current, the complete periphery of the core will be saturated regardless of the AC flux and provides the lowest secondary terminal voltage. In this way, the transformer voltage can be continuously regulated downward with increasing DC control.

The voltage regulation mechanism of a TAREX relies on the DC flux-biased magnetization of its core and the electromagnetically coupled dynamics inside the device. To understand the physics behind it, a thorough investigation was conducted through developing appropriate models, conducting analytical and numerical analyses, and validating with prototype testing.

First, an analytical model of the TAREX was developed for modeling of the dynamics and couplings between the electric and magnetic sides of the device. The analytical model was based on the reluctance-flux magnetic circuit model and the conventional electric circuit model (Steinmetz's model) of transformer. It is a set of algebra and differential equations consisting of the magnetic equivalent circuit equations and electric circuit equations. Solved together, the equations provide a fairly accurate description of how the winding voltage interacts with the DC control (i.e., the voltage regulation mechanism). The analytical model was then improved by the refinement of some key parameters/sub-models used in it, such as the winding leakage inductances and the DC controller model.

Second, numerical models of the TAREX were developed in commercial software tools (ANSYS Maxwell<sup>3</sup> and Plecs<sup>4</sup>) for modeling and cross-validation purposes. The finite element analysis (FEA) model developed in Maxwell was also used for modeling and analyzing the winding leakage inductances and improving the analytical model. The Plecs model was mostly used to study the interaction between the magnetic device and the DC controller.

Third, two bench-top prototypes were developed and tested for proof of concept and validation of analysis models. The prototypes were built on commercial small-capacity control or power transformers, which are easy to retrofit.

The biased magnetization in the TAREX may generate excessive harmonics and losses, which should be minimized not to affect the normal operation of the transformer. Finally, preliminary analyses were conducted to evaluate the harmonics that the TAREX may introduced to the grid, and possible measures to minimize the harmonics were briefly investigated.

### ***General information of the project***

The project started in October 2017 and most of the research work was completed by August 2019. It was supported under the Transformer Resilience and Advanced Components program by the Office of Electricity of the US Department of Energy with a total funding of \$500,000.

## **1.2 GENERAL FINDINGS**

1. The work conducted in this project showed that the voltage-regulating effect in a TAREX is the result of two major coupled electromagnetic processes simultaneously occurring under the DC flux-biased core magnetization. One is that the DC flux imposed by the controller saturates some parts of the core and shifts the magnetic induction between the AC windings (e.g., the primary and secondary for a 2-winding transformer). The other is that the DC flux increases the AC flux leakage in the windings and thus increases the leakage reluctances. In general, the increase of the leakage will result in higher losses because more stray fluxes possibly enclose their paths through the metal structure parts (e.g., core clamps, tie plates, and transformer tank) and generate excessive conduction and eddy losses. The issue is expected to be manageable because sophisticated measures in the transformer industry can reduce this type of losses. However, the loss factor should be considered during the design of a TAREX. The overall effect of the two processes is the reduction of the induced voltage in the winding not connected to a source. Therefore, the winding voltage can be magnetically regulated downward with increasing DC bias.
2. The voltage regulation of a TAREX can be well modeled by analytical and numerical methods. Analytical models based on the magnetic equivalent circuit (MEC) method with some improvements can provide fairly good representations of the voltage regulation process in a TAREX. FEA models of the TAREX allow more flexibilities in modeling magnetic details and thus give more accurate results. Modeling the leakage flux and inductance with the FEA model is more convenient. The analytical and FEA models developed in the project can both match testing results.
3. The magnetically regulated voltage was, for the first time, demonstrated on the prototypes developed in the project. Although that proved the concept of the TAREX, the voltage variation range obtained on the prototypes was limited (less than 5%). The prototypes were retrofitted from off-the-shelf commercial power transformers, which provide little room for reconfiguration and limit the regulation

---

<sup>3</sup> Maxwell 3D v.16.0, information of the newer version can be found at <https://www.ansys.com/products/electronics>

<sup>4</sup> Information of Plecs can be found at <https://www.plexim.com/plecs>

range that could be achieved. To effectively implement voltage regulation and achieve the desired range, a TAREX has to be carefully designed. The ratio of DC bias to AC excitation and the leakage inductance of the transformer winding are the key factors to consider.

4. The DC bias actually boosted the nonlinearity in the magnetization of the ferromagnetic core, resulting in an increased harmonics level in the induced voltage. Distortions on the secondary side voltage can be easily observed when DC bias was present during testing. One possible harmonics mitigation method was briefly investigated and found to be effective. It is based on the idea that injection of designed components in the DC control input can produce bias flux that possibly cancels part of the nonlinearity of the core magnetization and reduces the resulted harmonics.

### **1.3 RELEVANCE AND EFFECTS**

The modeling, prototyping, and testing work conducted in this project has established a clear understanding of the mechanisms of magnetically regulating transformer voltage. These efforts helped the authors understand the physics behind the technology of the TAREX. This work demonstrated, for the first time, the concept of continuous regulation of transformer voltage by controlling the magnetic field. The findings of the project will be valuable technical preparation for follow-up R&D efforts that may be seeking scaling up and commercialization. Success of the project can boost the confidence of potential future sponsors and reduce the risk for their investments. It will also benefit the research on similar or related technologies.

Successful development of this technology will enable and provide the level of voltage control necessary to operate the grid in a flexible and reliable manner. Without the need for mechanical switching, the TAREX is durable and resilient. It should also be more affordable than expensive high-power rating solid-state devices or tap changers.

The TAREX opens the door to a whole new R&D area that has great potentials of field application in real power systems since power transformers have been the backbone components of modern power systems, transmission, and distribution. It has the potential to solve the urgent challenges that the existing mechanical OLTC faces and fill the gaps between the conventional OLTC and next-generation technologies (e.g., solid-state transformers). It may enable the development of more flexible power transformers that can be used in a variety of situations that would otherwise require custom-designed transformers.

## 2. PROTOTYPES AND TESTING SETUP

The TAREX is an innovative use of the concept of SCR on conventional power transformers. Its configurations are relatively simple and straightforward, which allowed the authors to build prototypes before modeling and analysis. However, the modeling work requires prototypes for validation and improvement. Therefore, at the early stage of the project, the authors built two benchtop prototypes of a TAREX by retrofitting off-the-shelf low-rating transformers.

### 2.1 BENCHTOP PROTOTYPES

The first prototype was built on a TRIAD F-93X<sup>5</sup> control transformer. The F-93X transformer has a rating of 115:10/20/40 V, 50 VA. The transformer has a three-limb core stacked by silicon steel laminations of an E-I shape. The primary and secondary windings are wound on the center limb of the core in a concentric manner. Both the windings have multiple taps for achieving various voltage combinations. More details of the transformer are in APPENDIX A.

To build the prototype, two coils made of magnet wires (AWG 16 copper wire with brown insulation coating) were wound on the two side limbs as shown in Figure 2.1. Limited by the available space, in the core window between the outer winding and the side limbs, the number of turns of each coil was 22. The two coils were connected in a counter-series manner to form the DC winding. The terminals of the DC winding were connected to the DC source for imposing the bias flux.

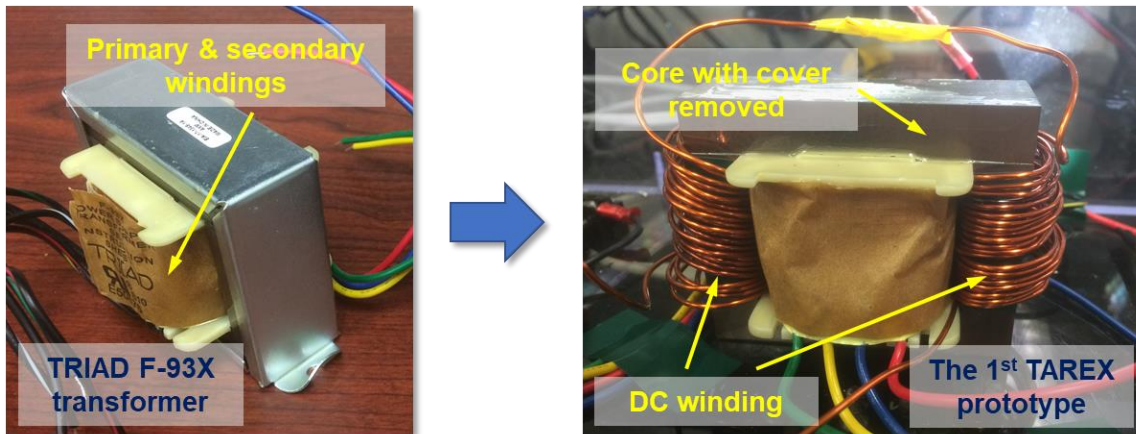


**Figure 2.1. The first prototype was retrofitted from a 115:10/20/40 V, 50 VA TRIAD transformer.**

The authors demonstrated the concept of TAREX on this prototype, regulating winding voltage by shifting core magnetization with DC bias. However, the small geometry and the low rating of the device prevented the authors from developing an accurate analysis model for it. Next, the authors built the second prototype.

The second prototype had a power rating of 500 VA, 10 times the first one. It was built on a TRIAD N-57MG<sup>6</sup> isolation transformer with a 1:1 voltage ratio at the nominal voltage of 115 V for both the primary and secondary windings as shown in Figure 2.2.

<sup>5</sup> <https://catalog.triadmagnetics.com/item/power-transformers/universal-chassis-mount-power-transformers/f-93x-1>

<sup>6</sup> <https://catalog.triadmagnetics.com/item/power-transformers/isolation-power-transformers/n-57mg-1>



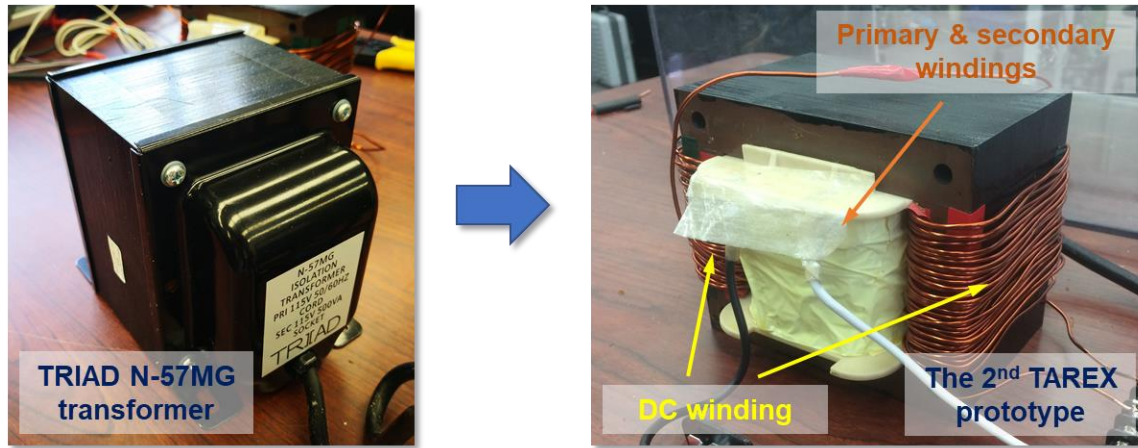


**Figure 2.2.** The second prototype was retrofitted from a 115:115 V, 500 VA TRIAD transformer.

## 2.2 TESTING AND PRELIMINARY RESULTS

The purposes of the testing on the prototypes were to prove the concept of the TAREX (regulating transformer winding voltage by using DC bias) and to validate the analysis models developed in the project and help understand the mechanism of the voltage regulation. To meet those needs, numerous transformer open-circuit tests and loaded tests were conducted on the two prototypes.

Figure 2.3 depicts the diagram of the test setup in general. The secondary winding being open-circuit or loaded determined the type of test. A TRIAD transformer was used to step down the wall outlet voltage ( $\sim 110$  V) to 20 or 40 V and supply the primary side of the TAREX prototype. Commercial DC supply sources were used to provide DC bias to the DC winding of the device. The voltage on the secondary winding was measured and the waveforms were recorded by using a Tektronix oscilloscope. The low voltage input to the prototype allowed the DC flux to easily dominate the AC flux and saturate the core (i.e., regulate the voltage). Additionally, the capacity limit of the commercial DC sources the authors used required lowering the input voltage to the prototype to achieve credible voltage regulation.



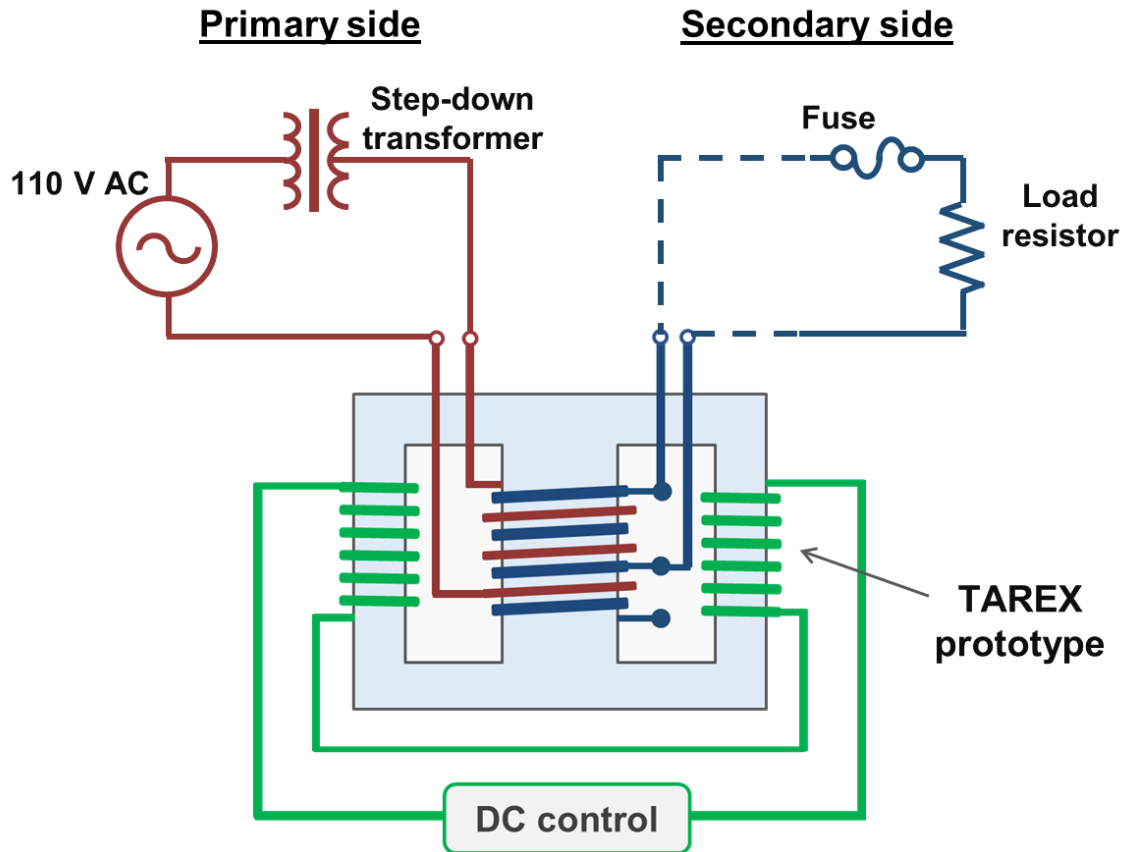


Figure 2.3. Diagram of testing for TAREX prototypes.

A photo of the testing setup taken during a loaded test of Prototype 1 is shown in Figure 2.4. On the right side of the figure, photos of the two commercial DC power supplies are shown. They were used in different tests based on the needs for the DC current capacity (KEITHLEY: 0~8 A; TENMA: 0~30 A).

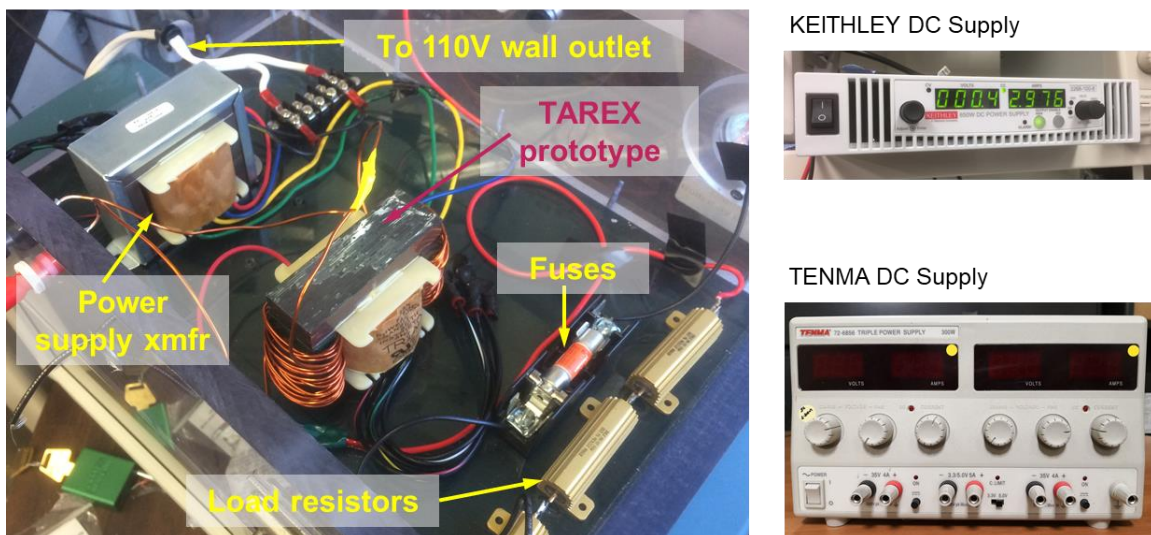


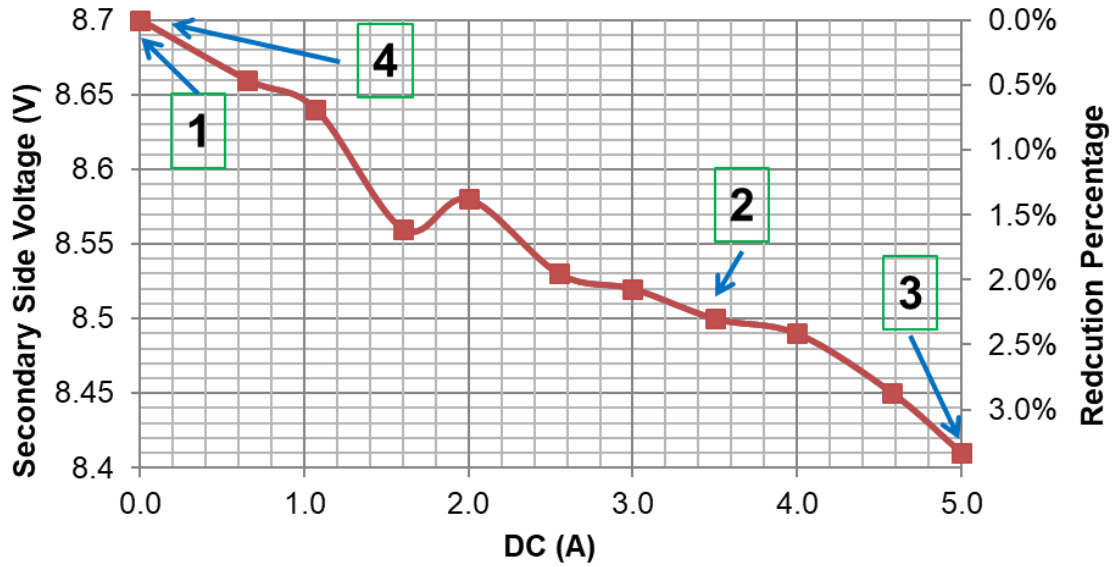
Figure 2.4. Test setup and DC power supplies.

### ***Preliminary test results***

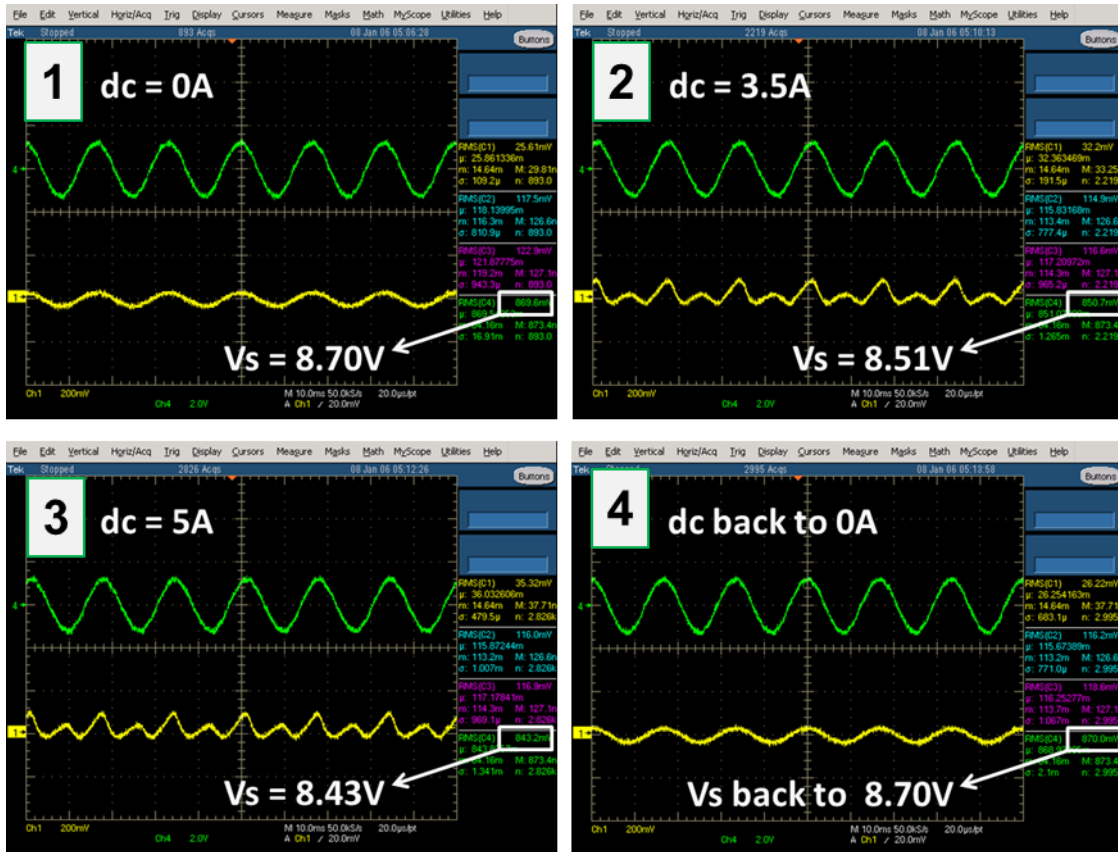
After the prototypes were built, some preliminary tests were conducted. These tests proved that the winding voltage of the transformer can be regulated (in a certain range) by controlling the DC flux imposed into the same ferromagnetic core of the transformer.

Figure 2.5 shows the results of an open-circuit test on Prototype 1. Figure 2.5 (a) shows that the secondary winding voltage drops by 3.3% over the DC control range of 0~5A. With the increase of DC supply, the nonlinearity of the core magnetization deepened, which can be reflected in the distortions of the secondary voltage and the induced voltage on the DC winding. The waveforms recorded at different test points of DC control can show this change as shown in Figure 2.5 (b). The test started at Point 1, with zero DC and no obvious distortions. As the DC input increased, the secondary winding voltage dropped and the distortions occurred, especially in the induced voltage on DC winding (Points 2 and 3). Once the DC input returned to zero, the secondary voltage returned to the initial value (Point 4).

Similar results were obtained from the loaded tests and from the tests of Prototype 2, showing that the transformer winding voltage can be regulated by control the DC bias imposed to the core. They helped achieve the first goal of the project, proving the concept of the TAREX. The second goal, to understand the mechanism of the voltage regulation, will rely on the modeling and validation work introduced in the following sections.



(a) Voltage drop on the secondary winding with the DC control.



(b) Waveforms of voltages on secondary and DC winding at different levels of DC control.

**Figure 2.5. Results of an open-circuit test on Prototype 1 to show voltage regulation enabled by DC bias control.**

### 3. ANALYSIS MODELS OF TAREX

#### 3.1 OVERVIEW

In the power industry, the most commonly used models for conventional power transformers are the Steinmetz's model for electric circuit modeling and the MEC model for magnetic field and induction modeling. Although good for many applications, the two models were insufficient for modeling the TAREX because of the special core magnetization (biased by DC flux) and characteristics of the TAREX.

For the convenience of analysis but without loss of generality, the authors assumed that the transformer being modeled was a three-limb-core, shell-type, single-phase transformer as shown in Figure 1.1. This type of transformer is widely used in power systems and is an idea for implementing the TAREX configuration.

A typical circuit presentation of the Steinmetz's transformer model [10], [11] for this transformer is shown in Figure 3.1. The model is a time-domain presentation of the model with all the variables presented in simultaneous format. The winding currents  $i_1$  and  $i_2$  and the core magnetic flux density  $\Phi_c$  are the state variables.  $i_1$  and  $i_2$  are dependent in that  $i_1/i_2 = N_2/N_1$ , where  $N_1$  and  $N_2$  are the turns ratio of the primary and secondary windings of the transformer.  $r_1$  and  $r_2$  are the resistances of the windings.  $L_{l1}$  and  $L_{l2}$  are the corresponding leakage inductances.  $e_1$  and  $e_2$  are the induced voltages.

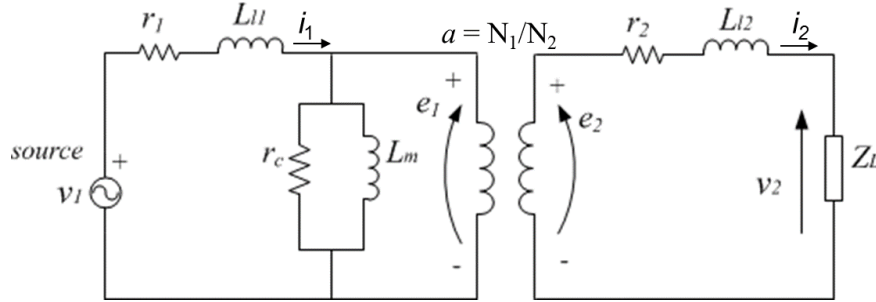


**Figure 3.1. The equivalent circuit model of a transformer.**

The time-domain equations of the model can be written as

$$\begin{aligned} v_1(t) &= r_1 i_1(t) + L_{l1} \frac{di_1(t)}{dt} + e_1(t) \\ v_2(t) &= -r_2 i_2(t) - L_{l2} \frac{di_2(t)}{dt} + e_2(t) \\ e_1(t) &= N_1 \frac{d\Phi_c(t)}{dt} \\ e_2(t) &= N_2 \frac{d\Phi_c(t)}{dt} = \frac{e_1(t)}{a} \end{aligned} \tag{3.1}$$

Solving these equations relies on the knowledge of the magnetic flux of the core, which cannot be immediately determined in the electric circuit model. Therefore, the authors also needed models that could describe the magnetization of the core to solve the problem. Numerous approaches to modeling exist for the electromagnetic process in a transformer [12]-[16], among which the MEC model [17], [18] is often used in practice. It is straightforward to understand for those who are familiar with electric circuit

analysis since the model is based on the concept of the magnetic reluctance, flux, and magnetomotive force (MMF), an analogy to the resistance, current, and voltage system in an electric circuit. Figure 3.1 depicts a MEC model for the transformer presented in Figure 1.1. In the model,  $R_1$ ,  $R_2$ , and  $R_c$  are the reluctances of the two side limbs and the center limb of the core.  $R_{L1}$  and  $R_{L2}$  are the leakage reluctance of the primary and secondary windings with respect to the core.  $F_1$  and  $F_2$  are the MMF of the two windings.  $\Phi_x$  ( $x = 1, 2, c, L1$ , or  $L2$ ) is the magnetic flux corresponding to each branch shown in the model.

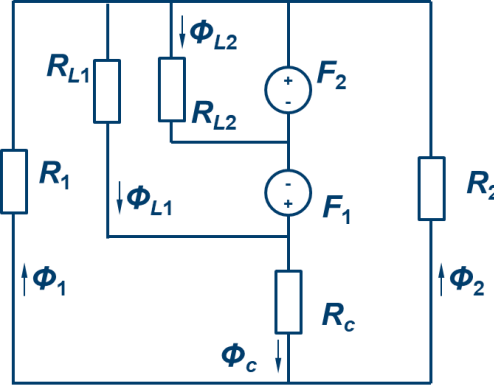


**Figure 3.1. An MEC model of the typical three-limb-core transformer shown in Figure 3.1.**

The magnetic reluctance ( $R$ ) of the core can be calculated by

$$R = \frac{l}{\mu_0 \mu_r A}$$

where  $l$  and  $A$  are the length and cross-sectional area of the mean flux path of the core,  $\mu_0$  is the magnetic permeability of free space, and  $\mu_r$  is the relative magnetic permeability of the core material. For ferromagnetic material, which the transformer core is built of,  $\mu_r$  is a function of the magnetic field. However, it is often treated as a constant in transformer modeling since transformers are designed for working in the linear region of core magnetization where  $\mu_r$  does not change very much. The leakage reluctance can be calculated by the same equation by using the  $l$  and  $A$  values of the corresponding leakage channel and  $\mu_r = 1$  (for air). The complicated part is how to determine accurate values of  $l$  and  $A$  because the exact geometry of the actual leakage channel for a winding is usually difficult to model. Some methods of leakage reluctance calculation are commonly used in practice and can provide relatively good estimation [11].

### 3.2 AN ANALYTICAL MODEL OF THE TAREX

The TAREX studied in this project uses DC flux to shift the transformer core magnetization so as to regulate the winding voltage. As introduced in Section 1, the uniqueness of the TAREX lies in the transformer induction process under the DC bias conditions, which is not a case that has been considered or analyzed for the normal operation of power transformers. To study and understand this special magnetization process, the authors developed an analytical model for the TAREX.

The model is based on the Steinmetz's and MEC models, with some tweaks to cover the DC bias conditions. The TAREX has two DC coils wound the two side limbs of the core to provide DC bias flux. This is not a configuration used on conventional transformers and thus had not been considered in existing transformer models. The DC winding is electrically isolated from the transformer windings. It interacts with the AC side of the device through the magnetic flux. The two DC coils are connected in a counter-series manner, generating DC fluxes circulating in a consistent direction in the periphery loop of

the core (side limbs and two yokes) as shown in Figure 3.2. This limb-yoke loop of the core will be saturated by the DC flux. The center limb will not see any DC flux. At any given time during an AC cycle, the direction of the AC flux will be the same as DC in half of the loop, while opposite in the other half. If the DC flux is comparable with the AC in magnitude, the right and left halves of the loop will be alternatively in saturation because of the AC cycles. If the DC flux overwhelms the AC, the loop will be in saturation all the time despite the AC cycle.

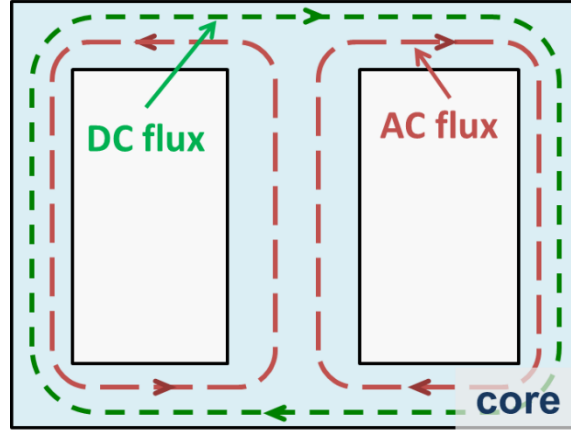


**Figure 3.2. Magnetic fluxes in the core of TAREX.**

With this knowledge of the fluxes, the MEC model of the TAREX was developed based on the model shown in Figure 3.1. Two MMF sources were added on the two outer branches as shown in Figure 3.3. Their polarity was set in such a manner that the induced DC fluxes are of consistent directions with respect to the aforementioned limb-yoke loop.

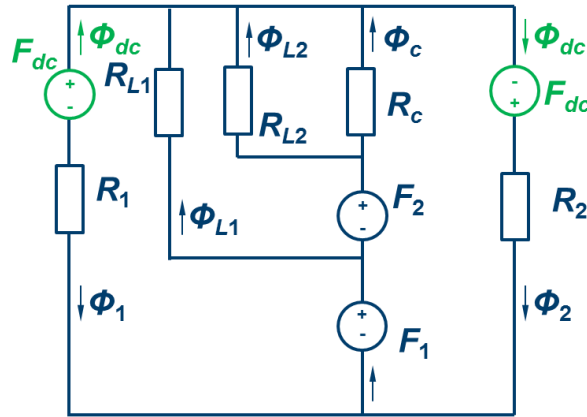


**Figure 3.3. One MEC model for TAREX with the MMF sources of DC.**

The magnetic circuit equations of the MEC model can be written as

$$\left\{ \begin{array}{l} F_{dc} + H_1 l_1 - \Phi_{L1} R_{L1} + H_c l_c = 0 \\ -F_1 + \Phi_{L1} R_{L1} - \Phi_{L2} R_{L2} = 0 \\ F_2 + \Phi_{L2} R_{L2} = 0 \\ F_1 - F_2 + F_{dc} + H_2 l_2 - H_c l_c = 0 \\ F_1 = N_1 i_1(t) \\ F_2 = N_2 i_2(t) \\ F_{dc} = N_{dc} I_{dc} \\ \text{B-H curve for interpolation} \end{array} \right. \quad (3.2)$$

where  $l_i$  ( $i = 1, 2$ , or  $c$ ) is the length of the magnetic path for the component of the core,  $i = 1$  or  $2$  is the left or right half of the limb-yoke loop,  $i = c$  is the center limb,  $H_i$  ( $i = 1, 2$ , or  $c$ ) is the magnetic field intensity of the corresponding part,  $\Phi_i$  ( $i = 1, 2, c, L1$ , or  $L2$ ) is the magnetic flux for each branch,  $R_{Li}$  ( $i = 1$  or  $2$ ) is the leakage reluctance of the primary or secondary winding, and  $F_i$  ( $i = 1, 2$ , or  $dc$ ) is the MMF for the primary, secondary, or DC winding. The B-H curve of the core material is known, and the B (magnetic flux density) or H field can be solved from each other by interpolating the curve. The DC supply,  $i_{dc}$ , and the instantaneous winding currents,  $i_1(t)$  and  $i_2(t)$ , are the inputs from the electric circuit model. If their values are known at a moment, Eq. (3.2) can be solved.

Here, the two leakage reluctances  $R_{L1}$  and  $R_{L2}$  are assumed to be constant. This assumption works well only to some degree because it is not consistent with the real case of the TAREX. The leakage reluctances in the TAREX are not constant. The analytical model can be improved to reduce this discrepancy. The improvement will be introduced in Section 4.3.

#### *Coupling with an electric circuit model*

The MEC model of the TAREX is coupled with the electric circuit model through the winding currents  $i_1(t)$  and  $i_2(t)$ , which need to be solved in the electric circuit Eq. (3.1). Therefore, the state of the device should be determined by solving all the electric and magnetic circuit equations together. Equation (3.1) can be combined into two differential equations as

$$\left\{ \begin{array}{l} v_1 = r_1 i_1 + L_{l1} \frac{di_1}{dt} + N_1 \frac{d\Phi_c}{dt} \\ v_2 = -r_2 i_2 - L_{l2} \frac{di_2}{dt} + N_2 \frac{d\Phi_c}{dt} \end{array} \right. \quad (3.3)$$

To solve the differential equations with algebra Eq. (3.2), Eq. (3.3) has to be discretized [19], [20]. By using the trapezoid method of integration, the discretization form of (3.3) can be written as

$$\left\{ \begin{array}{l} L_{l1}[i_1(t) - i_1(t - \Delta t)] + N_1[\Phi_c(t) - \Phi_c(t - \Delta t)] \\ + \frac{\Delta t}{2} [V_s(t) + V_s(t - \Delta t) - r_1(i_1(t) + i_1(t - \Delta t))] = 0 \\ L_{l2}[i_2(t) - i_2(t - \Delta t)] + N_2[\Phi_c(t) - \Phi_c(t - \Delta t)] \\ + \frac{\Delta t}{2} [(r_1 + r_{load})(i_1(t) + i_1(t - \Delta t))] = 0 \end{array} \right. \quad (3.4)$$

Equation (3.2) and (3.4) form the analytical model of the TAREX. One assumption made here is that the DC supply is an ideal current source, providing constant DC supply without being affected by the induced voltage on DC winding (i.e., of infinite internal impedance).

A MATLAB program was developed to implement the TAREX model. Figure 3.4 shows the flow of the program.

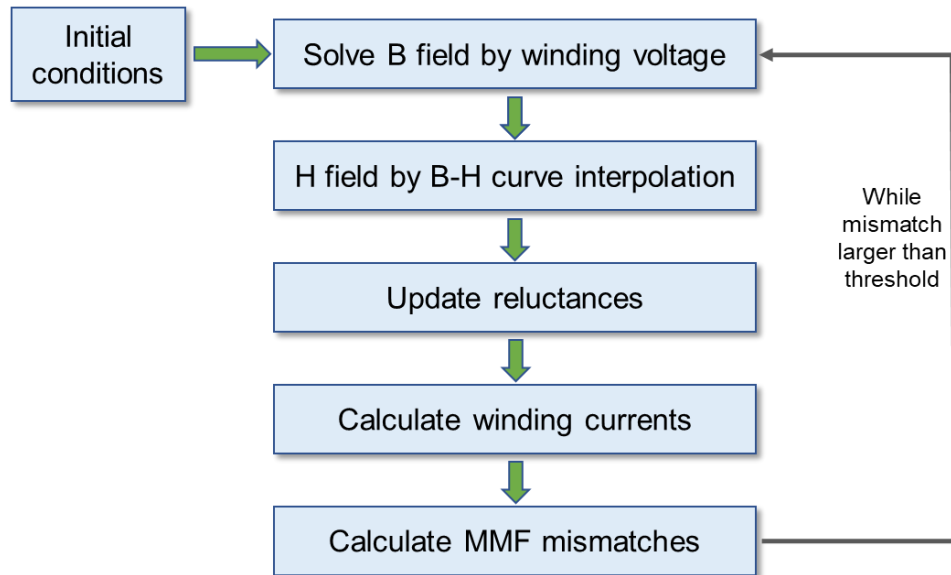


**Figure 3.4. Flow chart of the MATLAB program to implement the analytical model of the TAREX.**

The model can simulate the DC flux-biased magnetization of the core. Figure 3.5 shows the winding currents (top) and B fields calculated by using the TAREX analytical model for Prototype 1. The secondary winding of the prototype is assumed to be loaded with a resistance of 15  $\Omega$ .



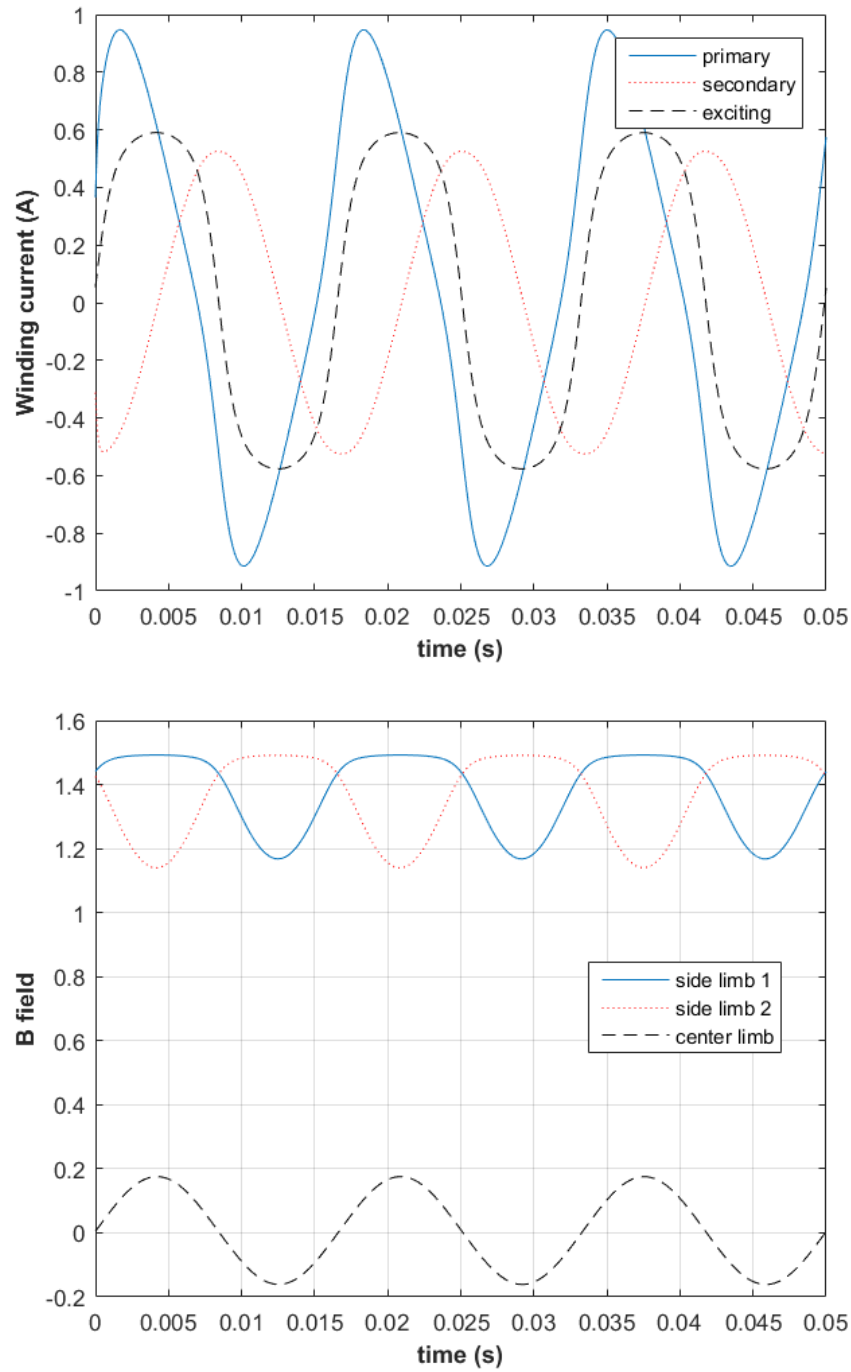


**Figure 3.5. (top) Winding currents of the three windings and (bottom) the B fields in the three core limbs calculated using the TAREX analytical model.**

Figure 3.6 shows the comparison of the results between the analytical model and testing. The analytical model did not succeed in matching the testing results. Some major limitations of the model resulted in its poor performance. These limitations are discussed in the following points, and the improvement of the model to address the issues is discussed in Section 4.

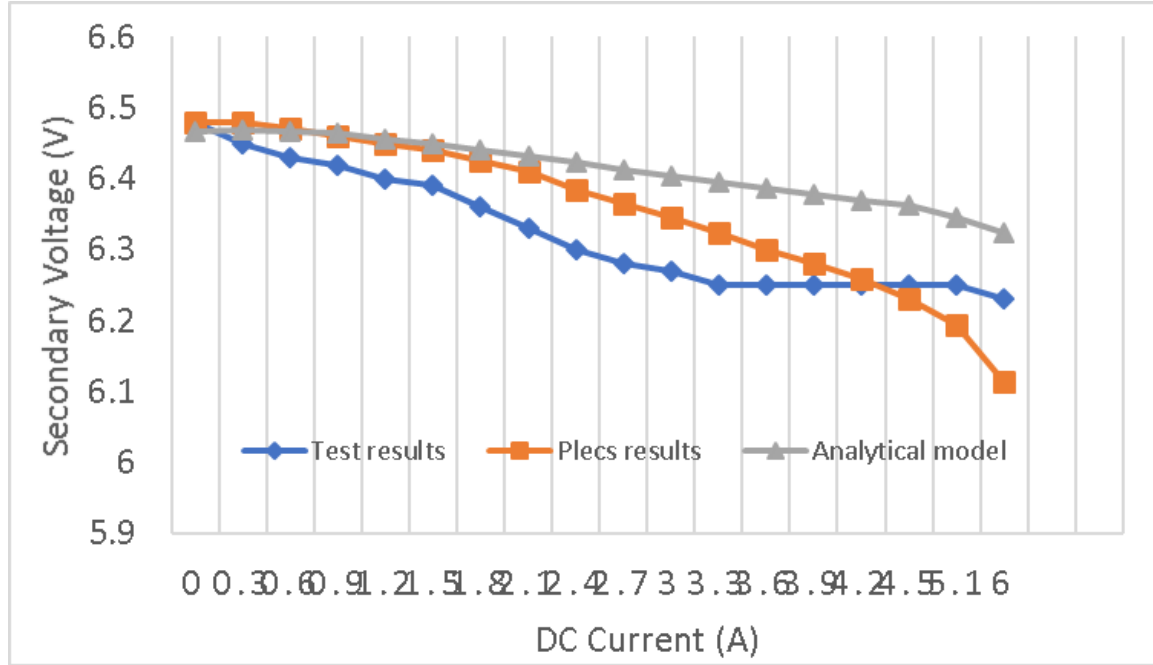


**Figure 3.6. Results comparisons between the analytical model, Plecs model, and testing (for prototype 1 with load resistance = 15  $\Omega$ ).**

### *Limitations of the analytical model*

1. The manufacturer does not provide the information of the core material of the TRIAD transformers that were used to develop the two prototypes. The authors assumed the core is stacked by M19 electrical steels, which are widely used to build commercial power transformers at the capacity level of the TRIAD ones. Thus, the authors adopted the B-H curve of M19 steel in the analytical and numerical analyses. However, the core material of the prototypes might not be M19, and using M19's B-H curve can cause inaccuracy. The improvement of this is discussed in Section 4.1.
2. As previously mentioned, the leakage reluctances are considered as constants in the developed analytical model. Although the assumption works well for the conventional transformer models, it is not satisfactory for the TAREX case. The DC bias flux imposed to the core changes the distribution of the leakage flux and thus affects the leakage reluctances. Assuming constant leakage reluctance may reduce the accuracy of the model.
3. The DC source is assumed to be an ideal current source, which is hardly the case in practice. The power electronics system of the DC supply has finite internal impedance and always interacts with the TAREX device through magnetic field induction. The interactions will affect the voltage regulation. Therefore, more detailed DC source model has to be considered and integrated into the TAREX model. The improvement of this part is discussed in Section 4.2.

### **3.3 FEA MODEL**

FEA-based simulations were conducted in the project for cross-validation with the analytical model and other models of the TAREX. FEA can model geometry details of the components (which is important for modeling magnetic devices such as the TAREX) and consider the nonlinear characteristics of component materials (e.g., the nonlinear magnetization of the ferromagnetic core material). These are all necessary for the TAREX case while difficult to realize by any analytical methods.

The authors developed 3D FEA models in ANSYS Maxwell for both TAREX prototypes. Figure 3.7 depicts the FEA model of Prototype 2. The geometries of the model were determined from measurements on the real device.

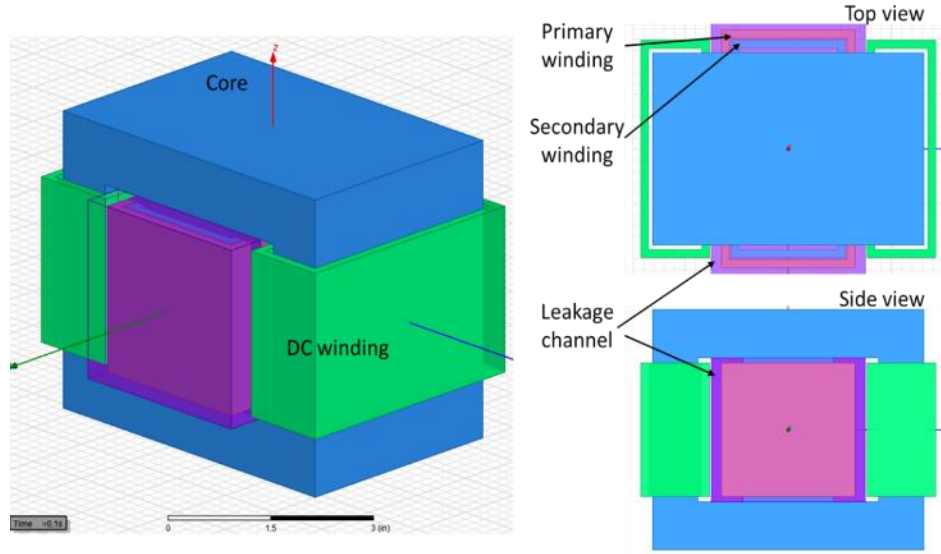


**Figure 3.7. The 3D FEA model of Prototype 2, showing the leakage channel defined to calculate the winding leakages.**

The model consists of 3D objects that represent the ferromagnetic core, primary winding, secondary winding, and DC winding of the prototype as shown in the figure. The magnetization characteristics of the core material were defined by the B-H curve of the material. The B-H curve of the M19 steel (APPENDIX A) was first used in the project and then replaced by the curve measured from the real device (see Section 4.1 for more details). The material for the windings was copper, one of the predefined materials in Maxwell. The leakage channel in the model was defined as the air volume (highlighted in purple) surrounding the center leg of the core and enclosing the primary and secondary windings. It was used to calculate the leakage reluctance of the windings and is discussed in Section 4.3.

The primary and secondary windings were wound around the center leg, and the two coils of the DC winding around the side legs. On each of the four winding objects, one “Coil” element (an embedded model element in Maxwell) was defined. They were assigned to the corresponding “Winding” elements (another type of model element in Maxwell, a Winding contains one or multiple Coils and one excitation source) that are defined for the primary, secondary, and DC windings. The two Coils of the DC winding were connected in the counter-series manner. An AC voltage or current source was assigned to each of the primary and secondary windings, depending on the circuit setup the authors wanted to test (e.g., open-circuit, short-circuit, or loading tests).

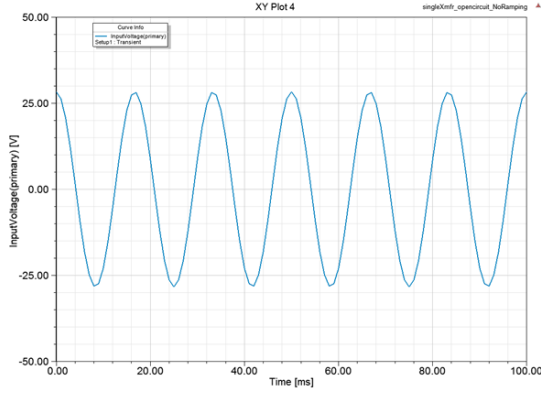
Table 3.1 shows the selection of source types for various tests.

**Table 3.1. Excitation source setups for different tests.**

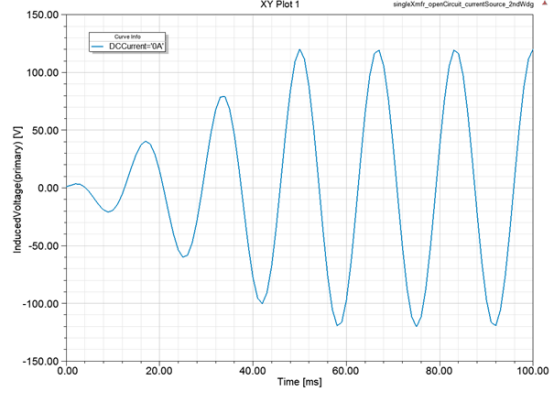
| Test                         | Primary winding        | Secondary winding                                    |
|------------------------------|------------------------|--|
| Open-circuit (on secondary)  | Voltage/current source | Current source, zero current                         |
| Short-circuit (on secondary) | Voltage/current source | Voltage source, zero voltage                         |
| Loading (on secondary)       | Voltage/current source | Voltage source, load impedance as internal impedance |

A DC source was assigned to the DC winding. Either voltage or current source can be used on the DC winding, depending on the DC controller model to be assumed. The current source is easier to setup because only the amplitude of the DC to be specified, whereas setting up the voltage source is not straightforward. One has to consider the induced voltage from the AC windings and its effect on the DC voltage source when using the voltage source on the DC winding. However, many of the power electronics-based DC sources, including the ones the authors used in this project, are actually voltage sources. In those cases, the voltage source model simulates the real physical processes more accurately and is more appropriate to be used.

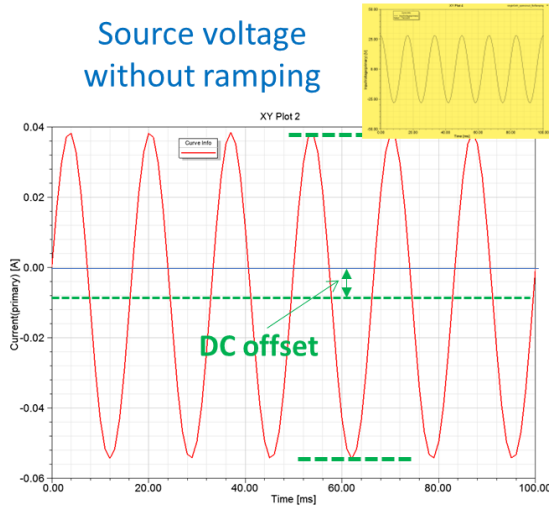
During the study, the authors found that how the AC excitations are applied affects the simulation results. If the AC voltage source (cosine wave) is directly applied to the winding at full amplitude (Figure 3.8 (a)), the induced current in the same winding will have a DC offset (Figure 3.8 (c)), which is not correct. Furthermore, the simulation results under this condition are incorrect. The reason for this issue is still unknown. The authors suggest it is caused by the internal calculation model of the software, and possibly by numerical calculation discrepancies from imposing a nonzero excitation suddenly at time zero. To solve the problem, the authors applied the source voltage through a ramping process (Figure 3.8 (b)), which gives a correct response in the induced current (Figure 3.8 (d)) and other analysis variables.



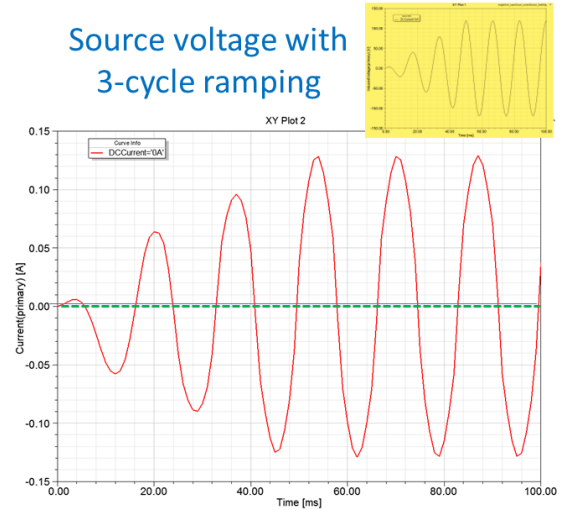
(a) Primary voltage without ramping – full magnitude instantaneously



(b) Ramping primary voltage – zero to full magnitude in 3 cycles



(c) A DC offset occurs in induced current, which is incorrect



(d) Symmetrical and not biased current after ramping completed

**Figure 3.8. Applying AC voltage source in the primary winding with or without ramping, and the corresponding induced currents in the same winding. AC voltage source without ramping may cause errors in simulation results.**

More details of how to set up the FEA models of the TAREX and how to apply the ramping AC voltage source are in APPENDIX B.

### 3.4 PLECS MODEL

Plecs is a commercial tool for power electronics systems simulation and integration [21]. It can also model the magnetic devices such as power transformers and inductors by using the Permeance-Capacitor approach for the MEC model. The Permeance-Capacitor approach is, in some sense, the dual method of the flux-reluctance approach introduced in Section 3.1. However, it has advantages over that approach in better representing the physics of magnetic induction in some cases [22]–[25]. In Plecs, it is convenient to create the permeance-capacitor models for magnetic devices (e.g., iron-core transformers/inductors) and the circuit models of the power electronics interfacing with the magnetic devices and thus analyze the interactions between them.

The authors used PLECS to model the TAREX device and the DC control together. Figure 3.9 shows the PLECS model of a TAREX system, with the magnetic components on top and the DC control on the bottom. In the magnetic component model, three major branches with magnetic permeances and equivalent capacitors in them represent the legs and yokes of the iron core. The permeances on the two outer branches were calculated for the side legs and the corresponding yokes of the core, and the permeance in the middle was for the center leg of the core. The side branch attaching to the center branch was for the leakage permeance, which represents the equivalent winding leakages. The four coil symbols in the model represent the windings/coils (primary and secondary windings and two DC coils) of the TAREX. Each of them has two terminals that interface with the external electric circuits. At the bottom of the main branches, three monitors of the derivative of magnetic flux observed the winding voltages. A current monitor in the DC winding loop watched the DC control. The DC control circuit was based on the design of the DC controller introduced in Section 4.2 (Figure 4.4). It is of a buck converter configuration.

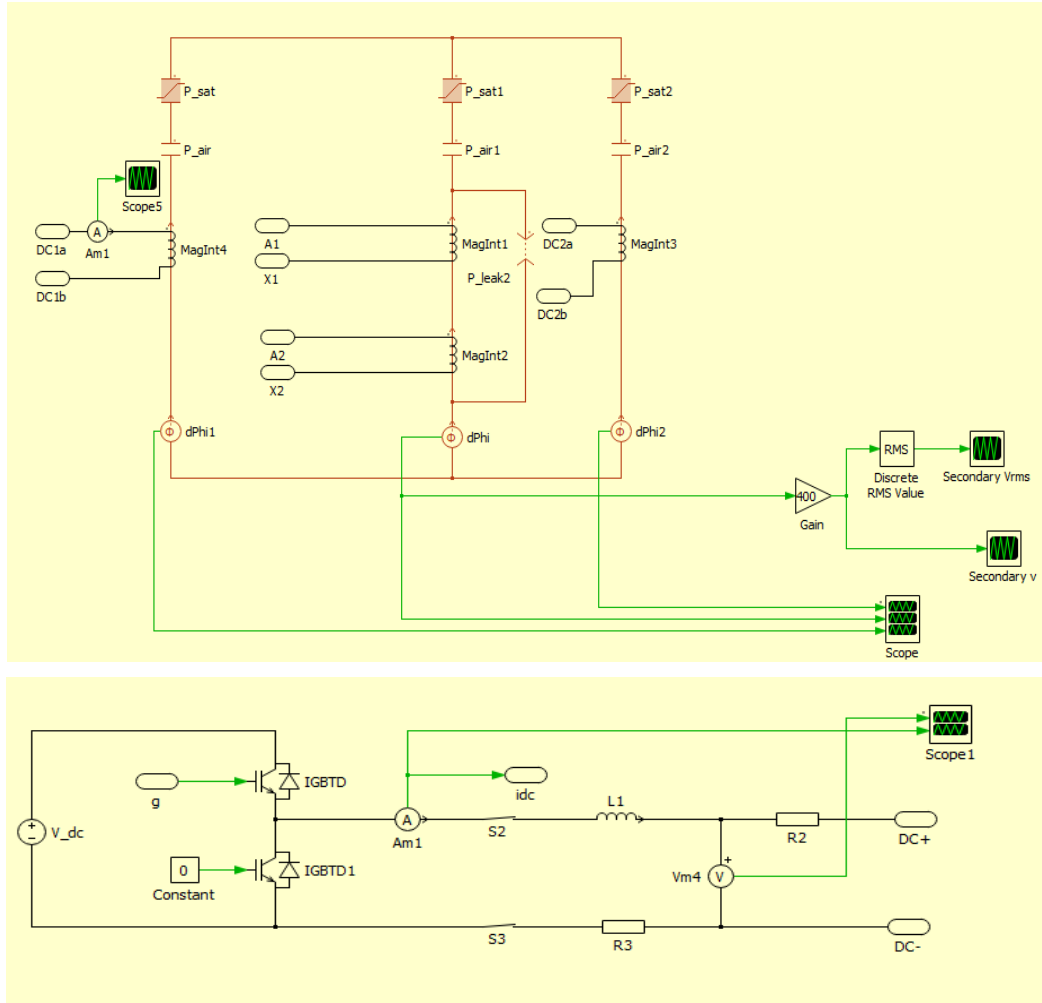


**Figure 3.9. A PLECS model of the TAREX.**

The PLECS model was used to simulate the voltage regulation of the TAREX for cross-validation with other analysis models and testing results. It was also used in the analysis for the harmonics of the TAREX. Figure 3.6 shows the comparisons between the results of the PLECS model, analytical model, and test. Although the PLECS results show some degree of agreement with the testing ones, the discrepancies between them are obvious. Some of the limitations of the PLECS model contribute to disagreement. The B-H curve used in PLECS (at least the version the authors used) to calculate the permeances was simplified to

a 2-segment linear model, which is too coarse to conduct the accurate quantitative analysis this study requires. Additionally, the model only accepts constant value for the leakage permeance, which is precalculated by the user. As the authors discussed in previous sections, the leakages of a TAREX are not constants. They are coupled with the AC excitations and the DC bias. Therefore, they are implicit variables that cannot be accurately determined in advance. A better practice to use the Plecs model is to obtain more accurate parameters such as the leakage permeances by using other approaches and use them to tweak the Plecs model for improved results. However, this still does not address the coarse B-H curve issue.

## **4. MODEL IMPROVEMENTS AND VALIDATIONS**

The development of the three analysis models (analytical, FEA, and Plecs) of the TAREX and their limitations are discussed in the last section. The models can be improved in several ways. In this section, efforts toward the improvement of the models are introduced.

### **4.1 IMPROVEMENTS BASED ON TESTING**

The qualities of the models the authors developed are all relying, more or less, on the accuracies of some basic model parameters. A team from the National Energy Technology Laboratory (NETL) helped the authors conduct some characterization tests to one TRIAD N57-MG transformer (the same type used to build Prototype 2) and refined the authors' knowledge of the device, which resulted in some improvements to the models of the TAREX. The tests done include

- Measurement of the number of turns of primary and secondary windings,
- Measurement of the B-H curve of the core, and
- Measurement of the leakage inductance.

A detailed report of the tests is in APPENDIX C.

The NETL team accurately measured the turns ratio (95:98) and B-H curve of the transformer. The results were used in the analytical and FEA models and improved their accuracy. Before the test, the authors assumed the core material of the prototypes to be M19 steel. The manufacture could not provide this information, so the authors had to assume based on the common industry practice. The NETL test showed that the magnetization characteristics of the core material were not the same as those of the M19 steel. Figure 4.1 shows the comparison between the B-H curves of the M19 steel and that measured from the prototype core. The difference is obvious, which implies the improvement of the models by using the new B-H curve.



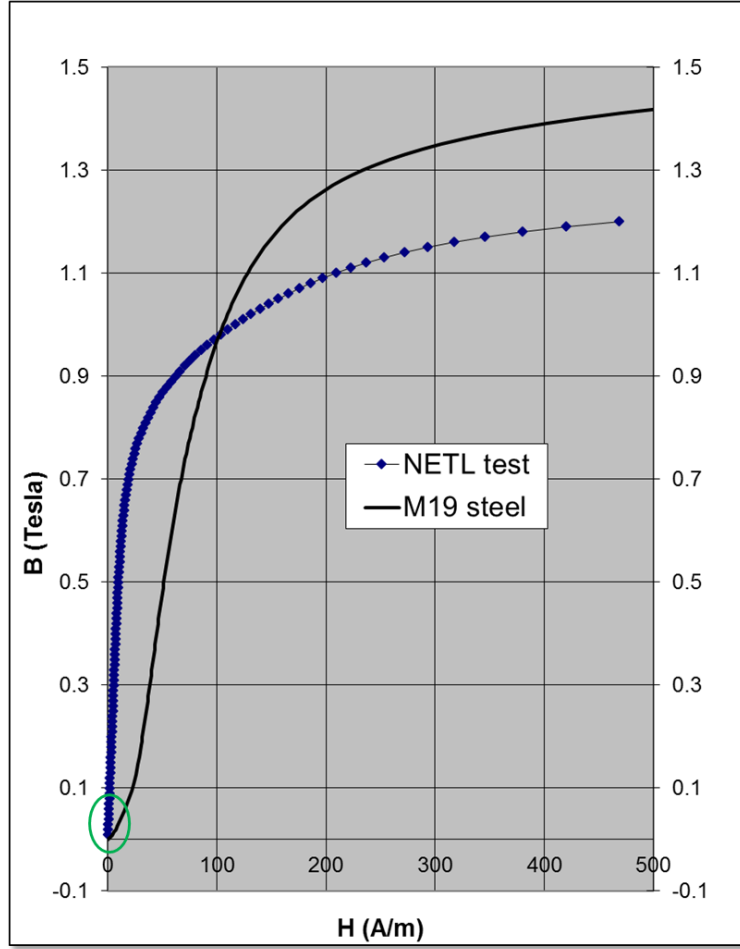


**Figure 4.1. B-H curve of M19 steel and the measured B-H curve of the core steel of Prototype 2.**

The authors then updated the B-H used in the analytical model and reran the simulations for validation. Figure 4.2 illustrates the improvement of accuracy by using the new (measured) B-H curve. The corresponding test was conducted on Prototype 2 with the secondary winding loaded with a resistor of 56  $\Omega$ . Overall, the voltage regulation curve for the new B-H curve was closer to the testing results compared with that for the M19 B-H curve, especially at the starting point, where there is no DC bias but the M19 result is obviously lower than the testing. The discrepancy is due to the slow ramping of the M19 B-H curve at the left-side end, highlighted by the green circle in Figure 4.1 (i.e., relatively small incremental permeability). The measured B-H curve has a much larger slope there.

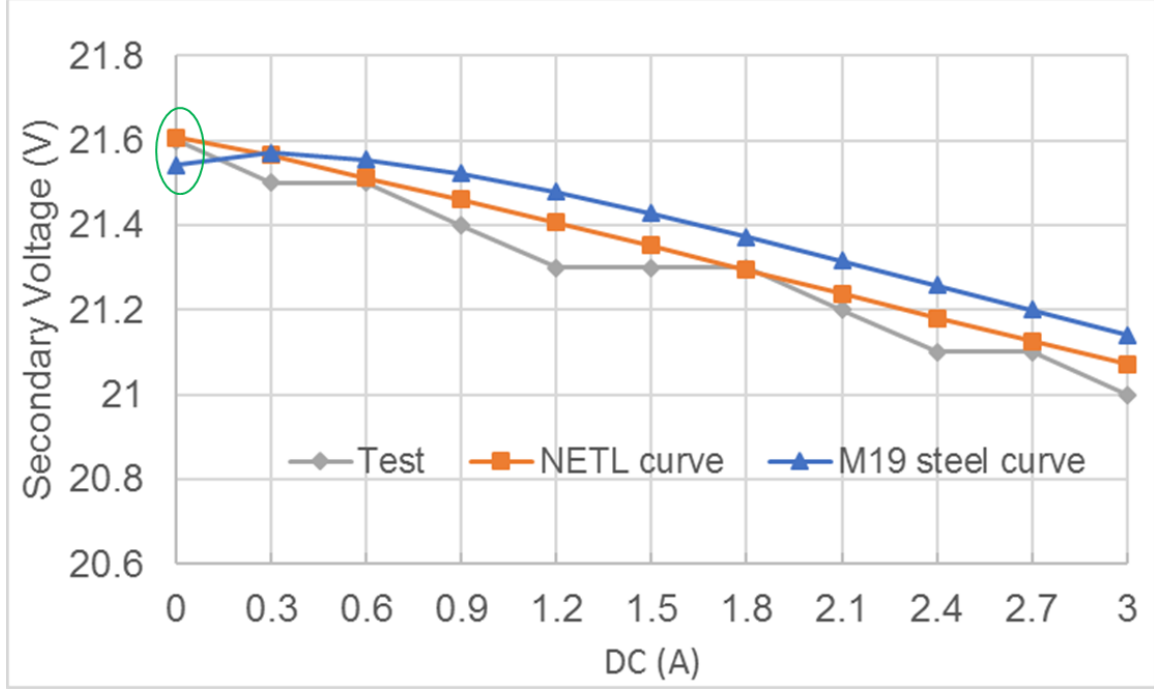


**Figure 4.2. Improvement by using the new B-H curve of the core measured by the NETL team (Prototype 2, loading resistor = 56  $\Omega$ ).**

#### 4.2 INTEGRATION OF DC CONTROL MODEL

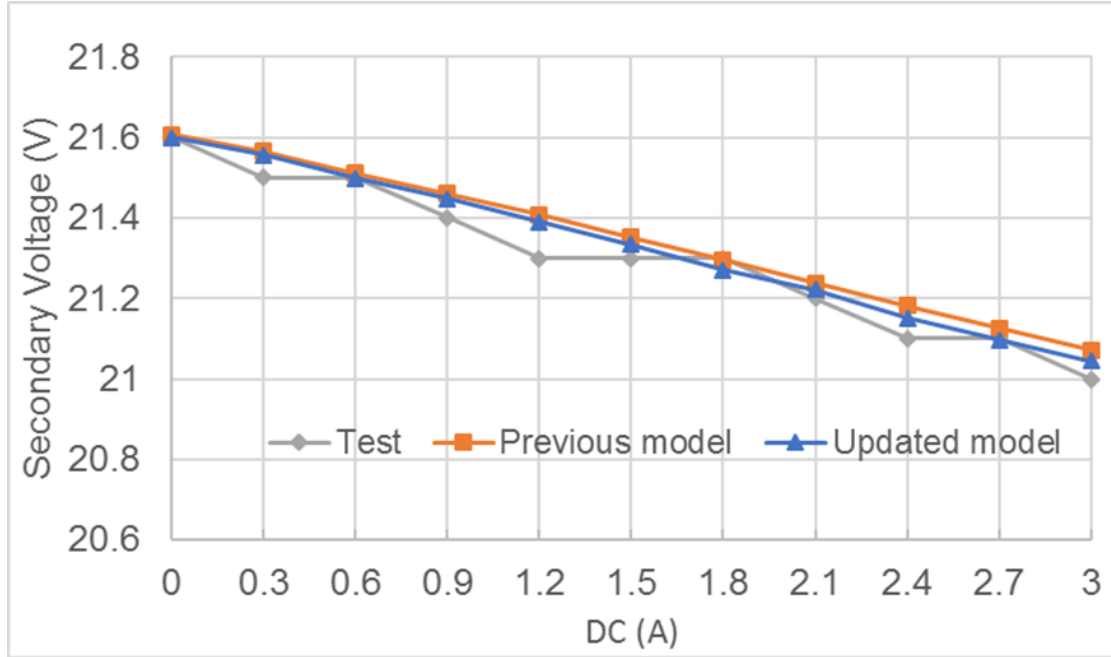
The DC control was previously assumed to be an ideal current source in the analytical model TAREX, which is probably not the most practical case. The assumption may cause discrepancies between the simulated and testing results. One immediate issue was that the voltage across an ideal current source was not defined, whereas in a real system, it is determined by the magnetic induction through transformer and DC windings.

The first improvement to make here was to use the voltage source model for the DC supply, replacing the current source model. This is a more realistic assumption because (1) most of the power electronics-based DC power supplies act as a voltage source that regulates its terminal voltage to control the output DC; and (2) the induced voltage on DC supply affects the terminal voltage (i.e., the output DC) by imposing ripples to it. The two effects are difficult to model if the DC supply is assumed to be a constant current source.

To implement the voltage source, the differential equation of the DC winding (4.1) is used.

$$(r_{dc1} + r_{dc2})i_{dcx} + (L_{dc1} + L_{dc2})\frac{di_{dcx}}{dt} = -N_{dc}\left(\frac{d\Phi_1}{dt} + \frac{d\Phi_2}{dt}\right) \quad (4.1)$$

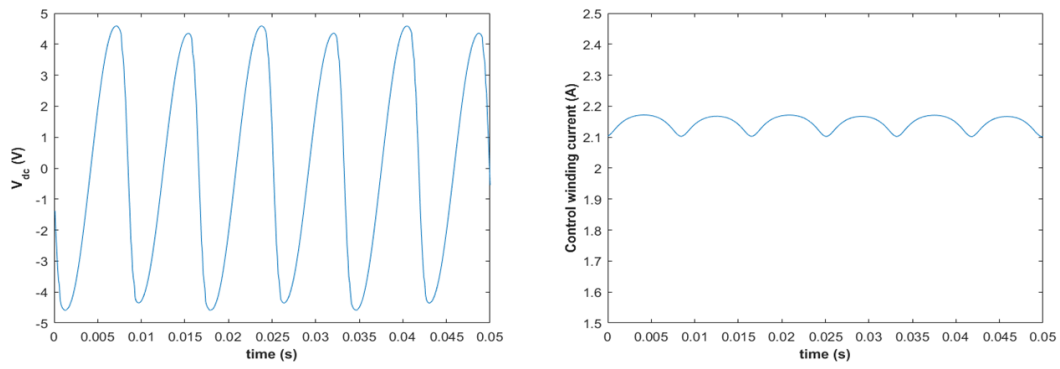
The discretization form of Eq. (4.1), obtained by using the same method as for Eq. (3.4), was then solved together with Eqs. (3.2) and (3.4). Implementing this change resulted in further improvements in the calculation of the voltage regulation as show in Figure 4.3.



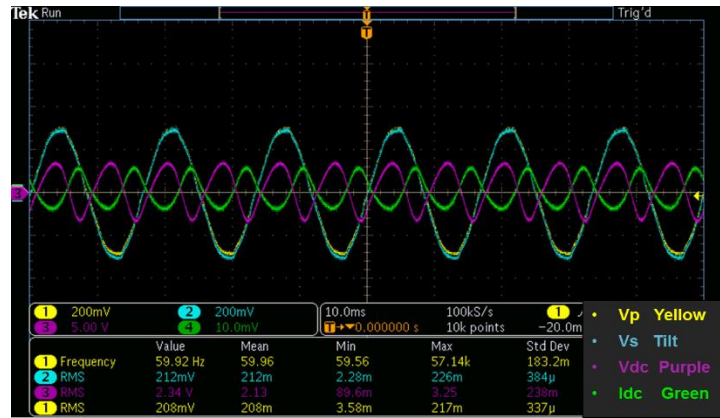
**Figure 4.3. Results of the winding voltage, updated model (using voltage source model) vs. the previous model (NETL curve in Figure 4.2).**

Figure 4.4 shows the comparisons between the calculated and testing results of the induced voltage (Figure 4.4 (a)) on the DC winding and DC current supply (Figure 4.4 (b)) for the same case shown in Figure 3.5. Consistent with the testing results, the calculated induced voltage had a fundamental frequency of 120 Hz. The magnitudes of the two were off by a factor, with ~3.3 Vrms for the calculated and 2.3 Vrms for the tested (purple curve in Figure 4.4 (b)). The DC currents were off by an even larger factor. The calculation shows a 2.1 A DC supply with 120 Hz ripples of <0.1 A magnitude. In the test results, the ripples in the DC supply were so large that they overwhelmed the DC. One theory to explain this is that the equivalent internal reactance of the DC source is usually capacitive, which together with the inductive reactance of the winding reduces the overall impedance in the DC control winding/circuit and results in large ripples. The authors tried the tests by using another commercial DC source and obtained similar results.

Besides the ideal voltage source, the authors also inspected a real DC controller and tried to integrate it with the analytical model. Figure 4.5 depicts the equivalent circuit and control loop diagram of a DC controller (DCC) the authors developed previously for the continuously variable series reactor (CVSR) project. The DC controller was designed for the application that is similar to usage conditions for the TAREX [26].  $Z_{dec}$  is the equivalent impedance of the DC controller looking into its output terminals. It can be calculated by the control parameters.  $V_o$  is the terminal voltage of the DC controller.



(a) Calculated by analytical model.



(b) Measured results.

Figure 4.4. Induced voltage on DC winding and ripples in DC supply, (a) calculations vs. (b) measurements.

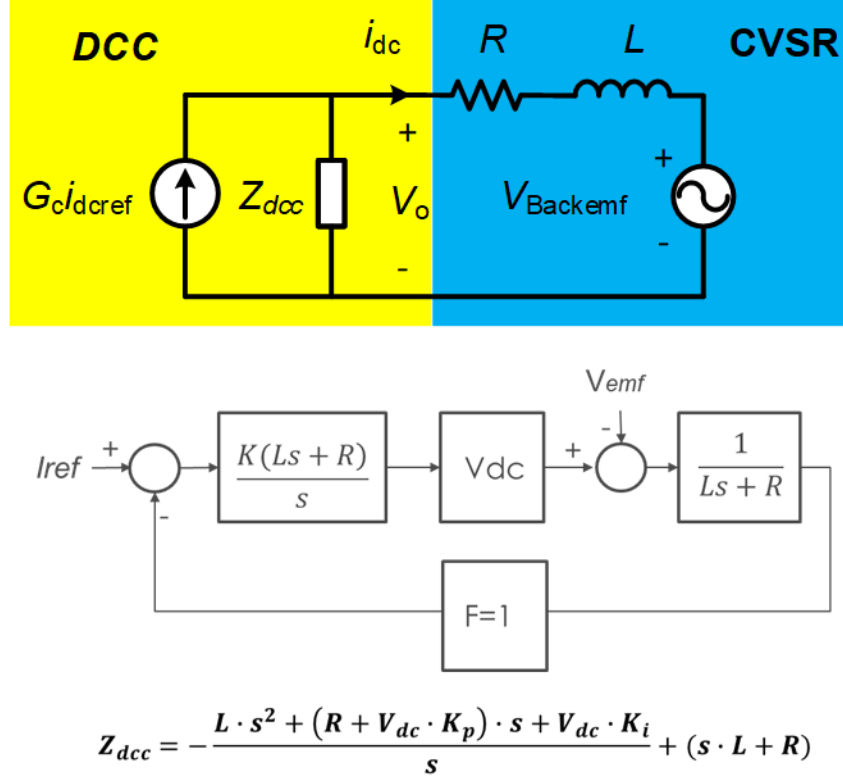


**Figure 4.5. (top) The equivalent circuit of the CVSR system and (bottom) frequency domain model of the DC controller (DCC).**

Based on the frequency-domain control model, the authors developed the time-domain model of the DC source by applying the inverse Laplace transform to the frequency-domain equation. The time-domain equation for DC current supply is

$$i_{dc}(t) = b_1 e^{-P_1 t} + b_2 e^{-P_2 t} + c_1 \cos(\omega t) + c_2 \sin(\omega t) \quad (4.2)$$

where

$$b_1 = KV_{dc} \left[ I_{ref} - \frac{FV_{e0}P_1}{(R - KV_{dc}FL)(P_1^2 + \omega^2)} \right]$$

$$b_2 = \frac{RV_{e0}P_2/L}{(R - KV_{dc}FL)(P_2^2 + \omega^2)}$$

$$c_1 = \frac{V_{e0}}{R - KV_{dc}FL} \left( \frac{KV_{dc}FP_1}{P_1^2 + \omega^2} - \frac{RP_2/L}{P_2^2 + \omega^2} \right)$$

$$c_2 = \frac{\omega V_{e0}}{R - KV_{dc}FL} \left( \frac{KV_{dc}F}{P_1^2 + \omega^2} - \frac{R/L}{P_2^2 + \omega^2} \right)$$

where  $R_{dc}$  and  $L_{dc}$  are the resistance and inductance of the DC winding. More details of the deriving process are in APPENDIX D. The time-domain equation can be solved in MATLAB. After some analysis, the authors realized that given the control scheme and parameter setup, this particular design of

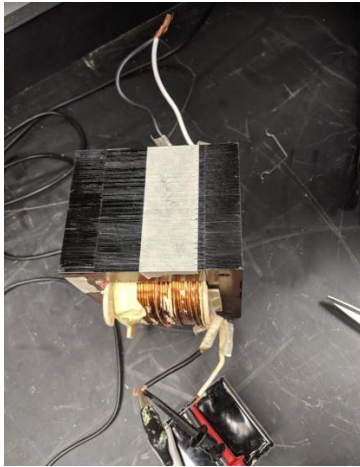
the DC source is the same as an ideal voltage source, and its time-domain response is the same as that obtained by using Eq. (4.1). The control scheme of the source was designed to main the terminal voltage  $V_o$  constant as long as it can. The  $V_o$  is determined by the induced voltage from the magnetic induction, which is the same as the case of using a constant voltage source model.

### 4.3 MODELING LEAKAGE INDUCTANCE

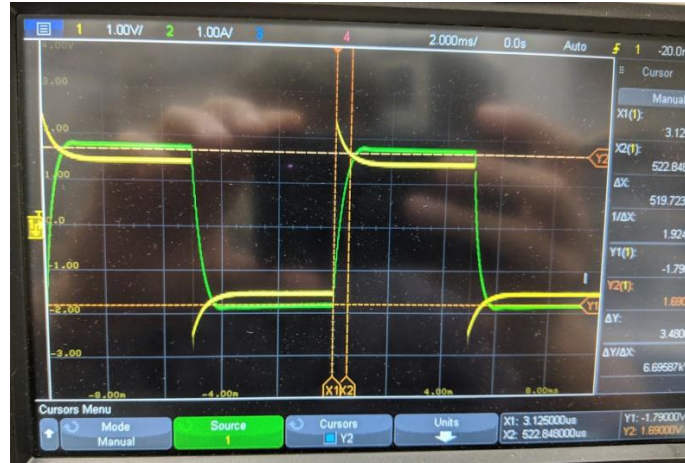
As mentioned in Section 3.2, the leakage inductance (i.e., reluctance) of the TAREX is affected by the presence of the DC flux in the core. It should not be treated as constant in the TAREX models if better accuracy is desired. The leakage flux encloses its path without coupling both of the primary and secondary windings. It heavily depends on the core magnetization and winding configuration. Modeling the leakage of transformer windings is often difficult. The empirical methods commonly used in transformer industry can estimate the steady state leakage to the accuracy level accepted by the industry [11], [27]–[30]. Most of the methods assume simplified distribution of the leakage flux and thus result in errors. A better approach is to use the FEA model to calculate the magnetic energy stored in the leakage channel to determine the leakage [15], [31], with the disadvantage of a heavy computation burden. The authors used the energy method in the project to study the leakage's effect on voltage regulation.

#### *Measurement of leakage inductance*

The NETL team conducted some initial tests to measure the winding leakages under the zero DC bias condition. The measurement gave the authors a baseline value of the leakage, which the authors used to benchmark the leakage calculation model. The test setup is shown in Figure 4.6 (a). With the secondary winding shorted, the primary winding's voltage and current were measured. Since the core loss skews the coil resistance (in the phasor plane) and affects the measurement, square waveform excitation was employed to do the inductance measurement.



(a) Test setup.



(b) Square-shape voltage excitation and induced current.

**Figure 4.6. (a) Test setup and (b) waveforms snapshot of the leakage measurement test (by the NETL team).**

The semi-square voltage excitation is shown in yellow in Figure 4.6 (b), and the corresponding current in green. The leakage inductance is estimated by using the induced voltage equation of an inductor:

$$V = L \frac{di}{dt}$$

The leakage inductance of the prototype transformer can be calculated as

$$L = V \frac{\Delta t}{\Delta i} = 2.03V \cdot \frac{520\mu s}{3.2A} = 320\mu H$$

The accuracy of the method was limited by the crude setup and the low excitation voltage, and the measurement error was estimated to be about 20%. Therefore, the total equivalent leakage inductance of Prototype 2 was measured as  $320 \mu H \pm 20\%$  ( $320 \mu H \pm 60 \mu H$ ). This result agrees with what the authors obtained by using the FEA method.

### ***Energy-based leakage model***

Modeling the leakage inductance was done to understand its effect on the voltage regulation of the TAREX. The authors used the magnetic energy approach to calculate the winding leakages. The magnetic energy stored in the leakage channel was calculated in the FEA model, and the leakage inductance was determined by using

$$W = \frac{1}{2} L_l I^2 = \frac{1}{2\mu_0} \int_{leakage\ channel} B^2 dV \quad (4.2)$$

As shown in Figure 3.7 (the 3D FEA model of Prototype 2), the leakage channel was defined as an air volume enclosing both the primary and secondary windings but excluding the center leg of the core. The magnetic field and energy were calculated in the transient simulation solver in Maxwell. The leakage inductance was calculated based on the induced current values at the selected time points. The energy corresponding to the leakage calculation was obtained in post-processing by integrating the energy over the volume of the leakage channel.

The calculation results of the leakage inductances for the short-circuit and open-circuit tests are shown in the following two tables (without any DC bias in both the simulations). The simulated short-circuit test result agreed very well with the results of the real tests (also in short-circuit configuration) done by the NETL team ( $312 \mu H$  vs.  $\sim 320 \mu H$ ).

|   |  | DCCurrent='0A'         |                        |                                   |
|---|--|------------------------|------------------------|-----------------------------------|
| Simulated short-circuit tests<br><br>(2 V cosine wave voltage<br>excitation on primary,<br>secondary shorted) | Time [ms]                              | Magnetic<br>Energy (J) | Induced<br>Current (A) | Leakage<br>Inductance ( $\mu H$ ) |
|   | 142                                    | 0.026722               | -13.0885               | 312.0                             |
|   | 146                                    | 0.044484               | -16.8888               | 311.9                             |
|   | 150                                    | 0.018764               | 10.9675                | 312.0                             |
|   | Average leakage inductance ( $\mu H$ ) |                        |                        | 312.0                             |

**Simulated open-circuit tests**

(120 V cosine wave voltage  
excitation on primary,  
secondary open)

|                                 | DCCurrent='0A'      |                     |                         |
|---------------------------------|---------------------|---------------------|-------------------------|
| Time [ms]                       | Magnetic Energy (J) | Induced Current (A) | Leakage Inductance (μH) |
| 92                              | 7.25E-07            | -0.0583             | 426.3                   |
| 96                              | 3.65E-06            | -0.12534            | 464.9                   |
| 100                             | 3.13E-07            | 0.03762             | 441.8                   |
| Average leakage inductance (μH) |                     |                     | 444.3                   |

***Affecting factors***

Several factors may directly affect the leakage inductance such as the DC bias and winding geometries. Imposing DC bias will increase the leakage flux around the windings (i.e., the leakage inductances). The following table shows the increase of the leakage inductance when a 10 A DC was applied in the control winding in a short-circuit test in an FEA simulation.

|           | DCCurrent='0A'      |                     |                         | DCCurrent='10A'     |                     |                         |
|-----------|---------------------|---------------------|-------------------------|---------------------|---------------------|-------------------------|
| Time [ms] | Magnetic Energy (J) | Induced Current (A) | Leakage Inductance (μH) | Magnetic Energy (J) | Induced Current (A) | Leakage Inductance (μH) |
| 142       | 0.027               | -13.09              | 312.0                   | 0.027               | -12.18              | 370.8                   |
| 146       | 0.044               | -16.89              | 311.9                   | 0.045               | -16.03              | 351.4                   |
| 150       | 0.019               | 10.97               | 312.0                   | 0.020               | 11.87               | 281.3                   |
|           |                     |                     | 312.0                   |                     |                     | 334.5                   |

Shifting the leakage inductance for short-circuit test or loaded case requires a relatively large DC since the magnetic flux due to the AC is strong and requires more DC flux to impose credible bias. Figure 4.7 shows that the leakage inductance increases with the DC bias presence. The shifted leakage inductance contributes to the voltage regulation.



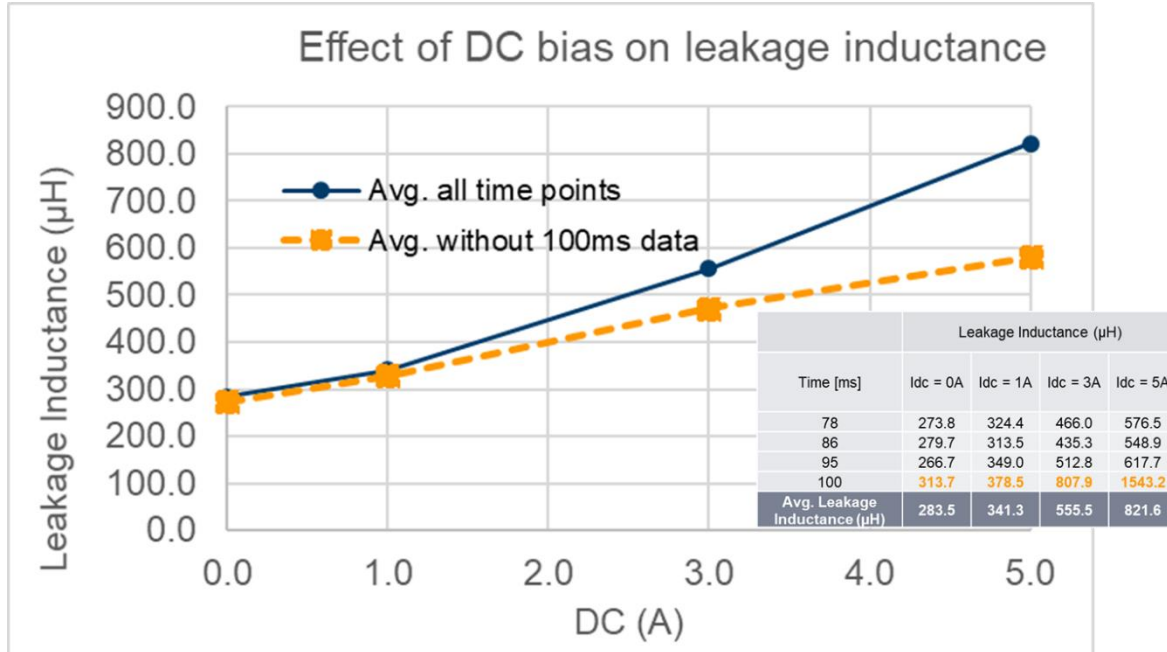
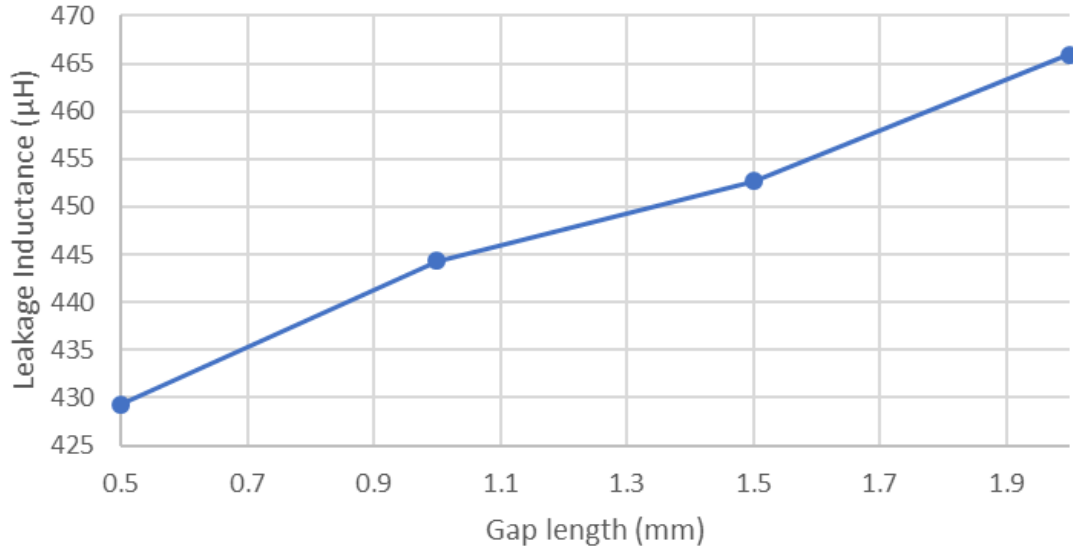


**Figure 4.7. The effect of DC bias on the leakage inductance.**

By using this method, a matrix of leakage inductance with respect to the combination of AC and DC excitation values can be generated and used in other TAREX models (e.g., analytical model), providing a look-up table for calculating the voltage regulation.

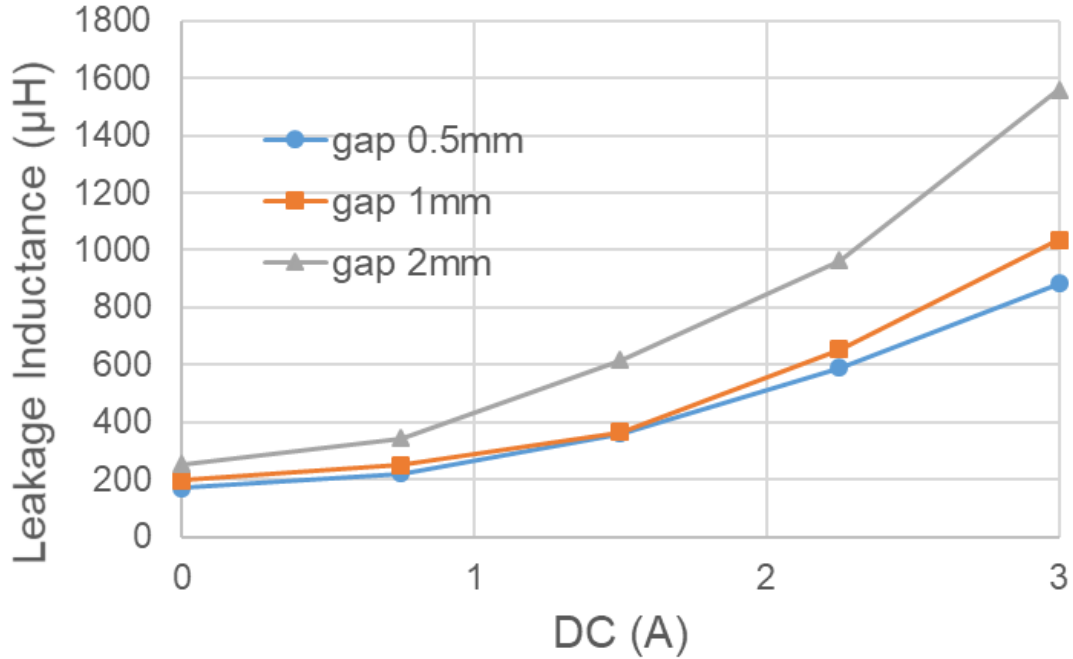
Generally, increasing the leakage will result in higher losses because more stray fluxes possibly enclose their paths through the metal structure parts of the device (e.g., core clamps, tie plates, and transformer tank), generating excessive conduction and eddy losses. Based on the analysis, the DC control can significantly increase the leakage (i.e., the level of stray flux) of the TAREX. However, the calculation results show that the change will not be off by orders of magnitude, so the increase of the stray flux is expected to be manageable. Sophisticated measures in the transformer industry can reduce the stray flux loss, such as cutting off the electrical conduction path in the metal structure by insulations between the metal parts and installing aluminum shielding plates. In future work, the excessive loss due to the DC bias should be quantitatively analyzed and modeled. The corresponding prevention measures should be integrated in the design of the TAREX.

Leakage inductance is an important design parameter of regular power transformers as well as the TAREX. Leakage inductances strongly depend on winding geometries. Given the previous analysis, the authors knew that the winding leakage determines, to some degree, the regulation range of a TAREX. Knowing the geometries' effects on the leakage helps optimize the TAREX design and achieve the desired voltage regulation range. Figure 4.8 shows the results of some brief analyses on the relationship between winding gap and leakage inductance of Prototype 2. The leakage inductance increased with the increase of the winding gap. Since the space for varying the winding gap length in a real transformer is usually limited, the tweaking range of the leakage inductance is also limited.



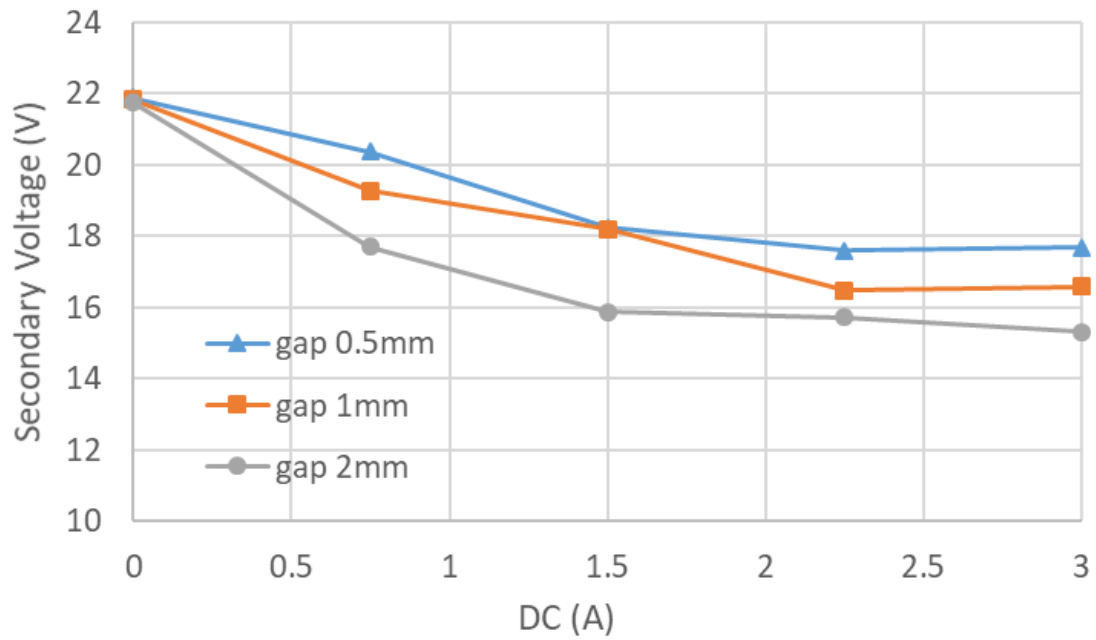
**Figure 4.8. Effect of winding gap on leakage inductance (by simulated open-circuit test on Prototype 2, DC = 0 A).**

Figure 4.9 shows the change of leakage inductances with the DC control for different winding gaps for a simulated load test on Prototype 2. The leakage inductance increased as the DC bias increased. A larger winding gap generally resulted in larger leakage inductance under the same DC bias level, which is consistent with the open-circuit case results shown in Figure 4.8. The monotonously changing characteristics (gap vs. leakage inductance) shown here may not apply to other TAREX designs. The authors have not conducted enough analysis in this project to exclude otherwise. The complexity of material magnetic characteristics and winding geometry might result in more complicated leakage inductance curves over different DC bias and winding gap conditions.



**Figure 4.9. Calculated leakage inductance with change of DC bias for different winding gaps (by simulated load test on Prototype 2, with a resistance load of 56  $\Omega$ ).**

The winding gaps' effects on the voltage regulation for the same case is shown in Figure 4.10. The regulation curves were calculated by using the circuit parameters obtained by FEA simulations and the transformer circuit model as shown in Figure 3.1. The instantaneous values of the winding currents, inductance matrix, and leakage inductances calculated in the FEA simulations were inserted into the circuit equation to determine the voltage across the 56  $\Omega$  resistor load. As expected, the load voltage dropped as the DC bias increased. A larger winding gap resulted in more voltage drop given the same DC bias range. The same argument made for Figure 4.9 applies here, as well. Not enough analysis has been done to ensure the winding gap and voltage regulation are of the monotonously changing relationship in all TAREX designs. Furthermore, the voltage drops given in Figure 4.10 are much larger than those obtained by the analytical model and testing. The reasons for this discrepancy are still unclear.



**Figure 4.10. Voltage regulation curves for different winding gaps (by FEA simulation results on Prototype 2, with a resistance load of 56  $\Omega$ ).**

## 5. HARMONICS ANALYSIS

The voltage regulation of TAREX depends on the nonlinear core magnetization due to the DC bias, which inevitably results in the increase of harmonics and distortion in the secondary voltage. If not mitigated, the harmonics may reach a level that is not acceptable in power grid applications. As the project proceeded, the authors realized that the harmonics mitigation has to be integrated into the design of the DC controller to make it practically viable. A thorough analysis on the harmonics characteristics of the induced voltage is critical for the design of a practically usable TAREX device.

When the core of a TAREX is operating in nonlinear magnetization, the major harmonics contents induced in the secondary voltage are the odd harmonics, and the third harmonics usually dominates. The cause of the harmonics and distortions is the magnetization nonlinearity induced by the DC bias. If some additional excitations that can cancel a portion of the nonlinearity are imposed, harmonics of the TAREX may possibly be reduced. This gave the authors some hints to a new harmonics mitigation approach by inserting carefully designed excitation components. Therefore, it is natural to insert those components into the DC supply.

The counter-series connection of the two DC coils forms the DC flux that circulated in the periphery loop of the core as shown in Figure 3.2. Therefore, only even-order AC components can be imposed on top of the DC supply in the DC control winding. All the odd-order AC components will be cancelled in the winding if the two DC coils are of good symmetry. Therefore, imposing even-order AC components in the DC supply is feasible for harmonics mitigation. If well designed, the imposed AC components in the DC supply can at least partly cancel the nonlinearity of the core magnetization induced by the DC bias and thus reduce the harmonics. In summary, the approach is to intentionally impose designed even harmonics ripples on top of the DC generated by the DC controller. The ripples will affect the core magnetization and counter some harmonics contents in the secondary winding. For optimal mitigation, the amplitude and phase angle of the imposed AC components have to be carefully determined.

The authors validated the concept of the mitigation approach and its effectiveness in a PLECS simulation. With an appropriate amount of the ripples imposed, the harmonics may be significantly reduced. Figure 5.1 shows the comparison of the secondary voltage waveform and harmonics contents before and after imposing the 2<sup>nd</sup> harmonics ripples in the DC output of the controller. With the mitigation method imposed, the 3<sup>rd</sup> and 5<sup>th</sup> harmonics in the secondary voltage significantly reduced and the distortion of the voltage waveform improved.

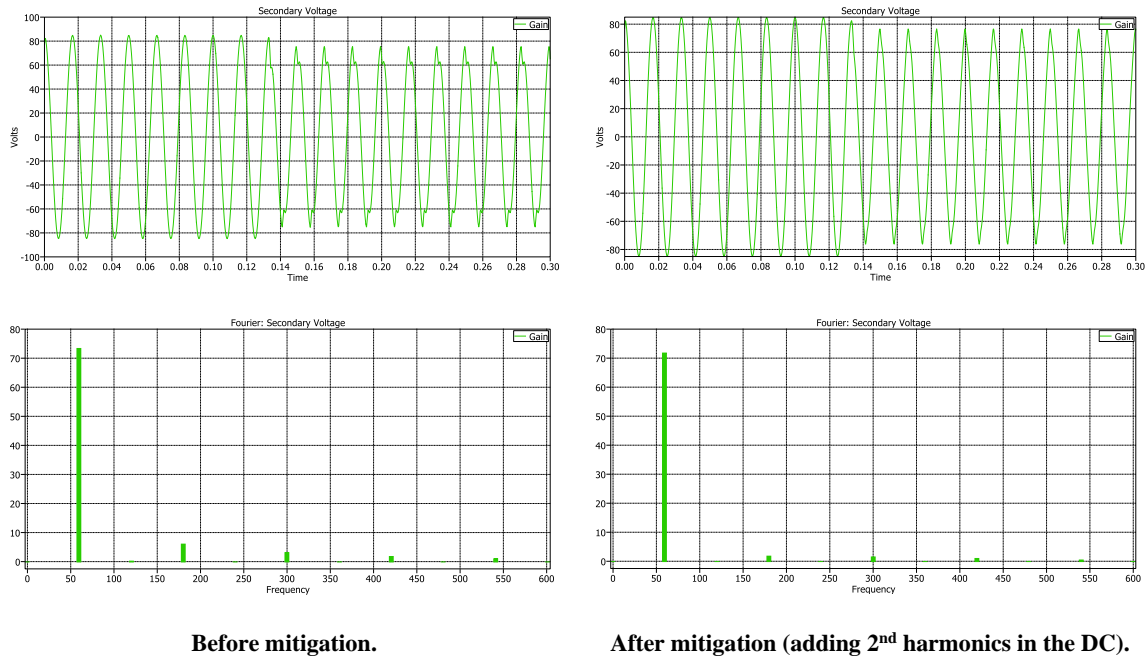
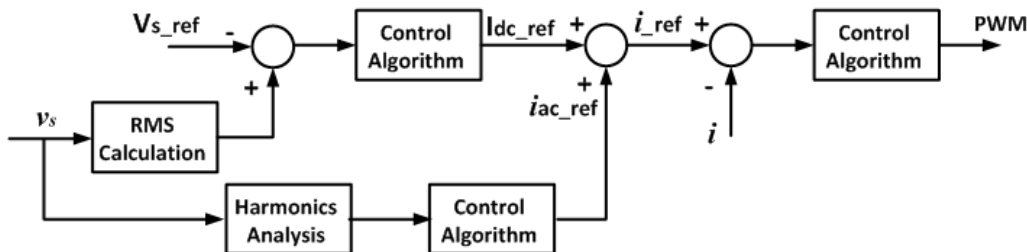


**Figure 5.1. Secondary voltage waveform and harmonics with/without the discussed mitigation method (imposing 2<sup>nd</sup> harmonics in the DC applied to the transformer).**



The idea of this harmonics mitigation approach can be extended to regular power transformers. Asymmetrical saturation is one type of abnormality that power transformers may encounter during the operation. It usually occurs when some DC components are present in the winding currents of the transformer, creating DC flux in transformer cores and shifting the core magnetization into asymmetrical saturation. In some sense, the process is similar to what occurs in a TAREX when the voltage is regulated by the imposed DC bias. The unexpected DC could be due to the geomagnetically induced current during a geomagnetic disturbance or the mono-polar operation of HVDC transmission lines nearby. The strong nonlinear core magnetization during the asymmetrical saturation significantly increases the harmonics level of the transformer. It is harmful for power grid operation and highly undesired. The uncontrolled harmonics can result in a number of severe problems, such as voltage collapse, transformer overheating, and false operation of protection equipment, and thus should be mitigated or avoided in any case.

The aforementioned harmonics mitigation approach can be adopted to address those issues of power transformers. The idea is to compensate the core magnetization, which is biased by the unexpected DC components flowing in the transformer windings (primary or secondary). To realize the compensations, an additional winding will be wound on the transformer core and connected to a compensating current source, similar to the DC winding in a TAREX (see Figure 1.1). The current source will be controlled to apply appropriate amount of current to the added winding, creating the fluxes in the core to compensate the asymmetrically biased core magnetization and mitigate the induced harmonics. The applied compensating current may consist of a DC component, AC components with different frequencies, or a combination of both the DC and AC components. The specifications of the control current should be determined by the loading of the transformer and the magnitude of the DC bias.

The mechanism of harmonics reduction relies on the fact that the compensating current will induce fluxes in the transformer core, which can partially cancel the nonlinearity of the core magnetization caused by the DC components in the original (e.g., primary or secondary) transformer windings. Again, for good performance, the DC and AC components of the compensating current have to be carefully determined. The magnitude of the DC component and the magnitude and phase angle of the AC component of the compensation need to be calculated based on the transformer magnetization model.

The principle of the proposed approach has been validated in testing on a benchtop prototype. A compensating winding is wound on a 115/40 V control transformer as shown in Figure 2.2. A sinusoidal voltage of 20 Vrms combined with a DC offset of 3 V was applied to the primary winding of the transformer when its secondary winding was loaded with a 15  $\Omega$ /50 W resistor. Figure 5.3 shows the harmonics components of the secondary voltage with/without applying the 2.4V DC voltage to the compensating winding. The 2<sup>nd</sup> harmonics (the major harmonics component) in the secondary voltage significantly reduced (by over 50%) by the compensation.

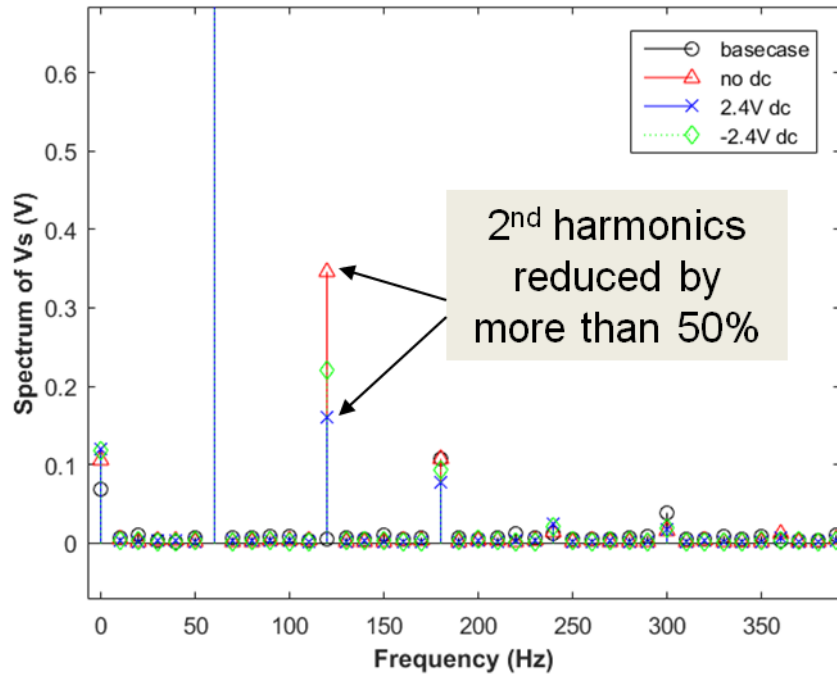


**Figure 5.3. Harmonics mitigation of a transformer under asymmetrical saturation (DC in primary winding) by using DC compensation in the additional control winding.**

One invention disclosure (ID number: 81915325) has been filed for this harmonics mitigation approach in power transformer applications.



## 6. CONCLUSIONS

The work conducted in this project has shown that the voltage-regulating effect in a TAREX is the result of two major coupled electromagnetic processes simultaneously occurring under the DC flux-biased core magnetization. One is that the DC flux imposed by the controller saturates some parts of the core and shifts the magnetic induction between the AC windings (e.g., the primary and secondary for a 2-winding transformer). The other is that the DC flux increases the AC flux leakage in the windings and thus increases the leakage reluctances. The linkage between the two processes is the nonlinear core magnetization. The overall effect of the two processes is the reduction of the induced voltage in the winding not connected to a source. Therefore, the winding voltage can be magnetically regulated downward with increasing DC bias.

The voltage regulation of a TAREX can be modeled by analytical and numerical methods. Analytical models based on the MEC method with some improvements can provide good representations of the voltage regulation process in a TAREX. FEA models of the TAREX allow better flexibilities in modeling magnetic details and thus give more accurate results. Modeling the leakage flux and inductance with the FEA model is also convenient.

The magnetically regulated voltage was, for the first time, demonstrated on the prototypes developed in the project. Although that proved the concept of TAREX, the voltage variation range obtained on the prototypes was limited (less than 5%). The prototypes were retrofitted from off-the-shelf commercial power transformers, which provide little room for reconfiguration and limit the regulation range can be achieved. To effectively implement voltage regulation and achieve the desired range, a TAREX has to be carefully designed. The ratio of DC bias to AC excitation and the leakage inductance of the transformer winding are the key factors to consider. In general, the amp-turns that the DC control/winding can provide should be comparable to that of the AC winding to allow enough DC bias for regulation. The turns of DC winding and the current rating of the DC source should be optimized in consideration of factors such as device size, copper loss, and DC source cost. For example, a large number of turns of DC winding requires a low rating of DC current, which results in higher copper loss.

The DC bias boosted the nonlinearity in the magnetization of the ferromagnetic core, resulting in an increased harmonics level in the induced voltage. Distortions on the secondary side voltage could be easily observed when DC bias was present during testing. One possible harmonics mitigation method was briefly investigated in the project. It was based on the idea that injection of designed components in the DC control input can produce a bias flux that possibly cancels part of the nonlinearity of the core magnetization and reduces the resulted harmonics.

The life cycle cost of power transformers with mechanical tap changers can range from \$20 to \$40/kVA, which is relatively high compared with the cost for regular power transformers (\$10–\$15/kVA). The solid-state transformer should be more expensive than the tap changers (transformer) because of the high cost of the high-rating power electronics. The TAREX is expected to be more competitive than those technologies in terms of cost. It requires only a low-rating power electronics system for regulation. The cost for the additional material and losses for the DC control will not be substantial (estimated less than \$5/kVA) compared with the cost of regular power transformers. Therefore, the overall cost of TAREX is reasonably expected to be a little higher than that for regular power transformers but much lower than for tap changers and solid-state transformers. However, the scale of the prototypes developed in the project may be too small to justify the cost advantage of TAREX. The economic benefits of TAREX is left for future studies.

Other efforts can be conducted in the future to improve the understanding of TAREX and facilitate scaling up the technology. They may include the following:

- Thermal and loss analysis to understand the thermal characteristics and excessive loss under DC bias conditions; identification of the optimal prevention measures of excessive loss if necessary;
- Optimal design for enough regulation range and good control sensitivity; and
- Close collaboration with manufacturers when developing a large-scale device to solve unexpected design and engineering issues.

All the work conducted in this project was based on the single-phase model of the TAREX. Expansion to a three-phase device also needs to be studied. A three-phase TAREX may be realized by three separate devices for a bank, or a single integrated device. The single device design will probably be of five-legged core configurations because the DC bias may require additional paths (legs) to circulate and saturate the core. One possible issue the three-phase TAREX may encounter is whether the voltage regulations for the three phases are symmetrical and balanced. If not, a separate control for each phase may be required. The economic benefits for doing that should be justified.

## REFERENCES

- [1] C. K. Gan, C. Y. Lau, K. A. Baharin, and D. Pudjianto, "Impact of the photovoltaic system variability on transformer tap changer operations in distribution networks," *CIREN - Open Access Proceedings Journal*, vol. 2017, no. 1, pp. 1818–1821, 2017.
- [2] D. Nguyen, P. Ubiratan, M. Velay, R. Hanna, J. Kleissl, J. Schoene, et al., "Impact Research of High Photovoltaics Penetration Using High Resolution Resource Assessment with Sky Imager and Power System Simulation," *CSI RD&D3 Subtask 4.3 Final Report*, Nov. 2015.
- [3] "On-Load Tap-Changers types UCC and UCD with motor-drive mechanism type BUE - Installation and Commissioning Guide," *ReadKong*, [online] Available: <https://www.readkong.com/page/on-load-tap-changers-types-ucc-and-ucd-with-motor-drive-4345189>
- [4] Boyajian, A., "Theory of D-C. Excited Iron-Core Reactors and Regulators," *Transactions of the American Institute of Electrical Engineers*, vol. XLIII, pp. 919–936, 1924.
- [5] H. S. Kirschbaum and E. L. Harder, "A Balanced Amplifier Using Biased Saturable Core Reactors," *Transactions of the American Institute of Electrical Engineers*, vol. 66, no. 1, pp. 273–278, 1947.
- [6] A. Dimitrovski, Z. Li, and B. Ozpineci, "Applications of saturable-core reactors (SCR) in power systems," *2014 IEEE PES T&D Conference and Exposition*, Chicago, Illinois, 2014.
- [7] A. Dimitrovski, Z. Li, and B. Ozpineci, "Magnetic Amplifier-based Power Flow Controller," *IEEE Transactions on Power Delivery*, vol. 30, no. 4, pp. 1708–1714, 2015.
- [8] "Magnetic Amplifier for Power Flow Control," *ARPA-E*, Project Coordinator: A. Dimitrovski, <http://arpa-e.energy.gov/?q=slick-sheet-project/magnetic-amplifier-power-flow-control>
- [9] A. Dimitrovski, "Power Flow Control Using Distributed Saturable Reactors," US PTO Application #PCT/US12/26111.
- [10] G. McPherson and R. D. Laramore, *An Introduction to Electrical Machines and Transformers*, 2nd Edition, Wiley, USA, 1990.
- [11] R. M. Del Vecchio, B. Poulin, P. T. Feghali, D. M. Shah, and R. Ahuja, *Transformer Design Principles: With Applications to Core-Form Power Transformers*, 2nd Edition, CRC Press, 2017.
- [12] N. D. Hatziaargyriou, J. M. Prousalidis, and B. C. Papadias, "Generalised transformer model based on the analysis of its magnetic core circuit," *IEE Proceedings C - Generation, Transmission and Distribution*, vol. 140, no. 4, pp. 269–278, July 1993.
- [13] J. A. Martinez and B. A. Mork, "Transformer modeling for low- and mid-frequency transients - a review," *IEEE Transactions on Power Delivery*, vol. 20, no. 2, pp. 1625–1632, Apr. 2005.
- [14] A. Rezaei-Zare, "Enhanced Transformer Model for Low- and Mid-Frequency Transients—Part I: Model Development," *IEEE Transactions on Power Delivery*, vol. 30, no. 1, pp. 307–315, Feb. 2015.
- [15] L. Cao, J. Zhao, and J. He, "Improved Power Transformer Model for DC Biasing Analysis Considering Transient Leakage Reluctances," *2006 International Conference on Power System Technology*, Chongqing, pp. 1–5, 2006.
- [16] H. Li, X. Cui, T. Lu, Z. Cheng, and D. Liu, "An improved magnetic circuit model of power transformers under DC bias excitation," *2010 Asia-Pacific International Symposium on Electromagnetic Compatibility*, Beijing, pp. 806–809, 2010.

- [17] J. Arrillaga, W. Enright, N. R. Watson, and A. R. Wood, "Improved simulation of HVDC converter transformers in electromagnetic transient programs," *IEEE Proceedings - Generation, Transmission and Distribution*, vol. 144, no. 2, pp. 100–106, Mar. 1997.
- [18] L. Qing, Z. Shihe, and S. Shuai, "Study of DC bias of power transformer based on UMEC model," *2015 7th Asia-Pacific Conference on Environmental Electromagnetics (CEEM)*, Hangzhou, pp. 65–68, 2015.
- [19] H. W. Dommel, "Digital Computer Solution of Electromagnetic Transients in Single-and Multiphase Networks," *IEEE Transactions on Power Apparatus and Systems*, vol. PAS-88, no. 4, pp. 388–399, Apr. 1969.
- [20] H. W. Dommel and W. S. Meyer, "Computation of electromagnetic transients," *Proceedings of the IEEE*, vol. 62, no. 7, pp. 983–993, July 1974.
- [21] J. Allmeling, W. Hammer, and J. Schönberger, "Transient simulation of magnetic circuits using the permeance-capacitance analogy," *2012 IEEE 13th Workshop on Control and Modeling for Power Electronics (COMPEL)*, Kyoto, pp. 1–6, 2012.
- [22] Y. Lee and M. Chow, "Modelling and teaching of magnetic circuits," *Asian Power Electron. J.*, vol. 1, pp. 15–20, 2007.
- [23] D. Hamill, "Gyrator-capacitor modeling: A better way of understanding magnetic components," *Proceedings of the IEEE Applied Power Electronics Conference and Exposition*, vol. 1, pp. 326–332, 1994.
- [24] R. W. Buntenbach, "Analogues between magnetic and electrical circuits," *Electronic Products*, pp. 108–113, Oct. 1969.
- [25] M. Young, A. Dimitrovski, Z. Li, and Y. Liu, "Gyrator-Capacitor Approach to Modeling a Continuously Variable Series Reactor," *IEEE Transactions on Power Delivery*, vol. 31, no. 3, pp. 1223–1232, 2016.
- [26] S. Zheng, J. Wang, F. Yang, F. Wang, L. M. Tolbert, and D. J. Costinett, "A DC controller for continuous variable series reactors (CVSRs)," *2015 IEEE Energy Conversion Congress and Exposition (ECCE)*, Montreal, Quebec, pp. 5786–5793, 2015.
- [27] J. H. Kuhlmann, "Physical concept of leakage reactance," *Electrical Engineering*, vol. 67, no. 2, pp. 142–146, Feb. 1948.
- [28] B. Tomczuk, "Three-dimensional leakage reactance calculation and magnetic field analysis for unbounded problems," *IEEE Transactions on Magnetics*, vol. 28, no. 4, pp. 1935–1940, July 1992.
- [29] B. Tomczuk, "Analysis of 3-D magnetic fields in high leakage reactance transformers," *IEEE Transactions on Magnetics*, vol. 30, no. 5, pp. 2734–2738, Sept. 1994.
- [30] F. de Leon and J. A. Martinez, "Dual Three-Winding Transformer Equivalent Circuit Matching Leakage Measurements," *IEEE Transactions on Power Delivery*, vol. 24, no. 1, pp. 160–168, Jan. 2009.
- [31] H. Fukumoto, T. Furukawa, H. Itoh, and M. Ohchi, "Calculating leakage reactance of 9-winding transformer using time-dependent 3D FEM analysis," *IECON 2015 - 41st Annual Conference of the IEEE Industrial Electronics Society*, Yokohama, pp. 004459–004464, 2015.

## APPENDIX A. PROTOTYPE PARAMETERS

**Table A-1. Parameters of the two TAREX prototypes.**

|                              | Prototype 1                   | Prototype 2   |
|------------------------------|-------------------------------|---------------|
| Core width                   | 3                             | 5.25          |
| Core height                  | 2.5                           | 4.375         |
| Core depth                   | 1                             | 3.5           |
| Window width                 | 0.5                           | 0.875         |
| Window height                | 1.5                           | 2.625         |
| Primary winding # of turns   | 1,150 (estimated)             | 95 (measured) |
| Secondary winding # of turns | 400 (estimated, 115/40 V tap) | 98 (measured) |

**Table A-2. B-H curve data of M19 steel.**

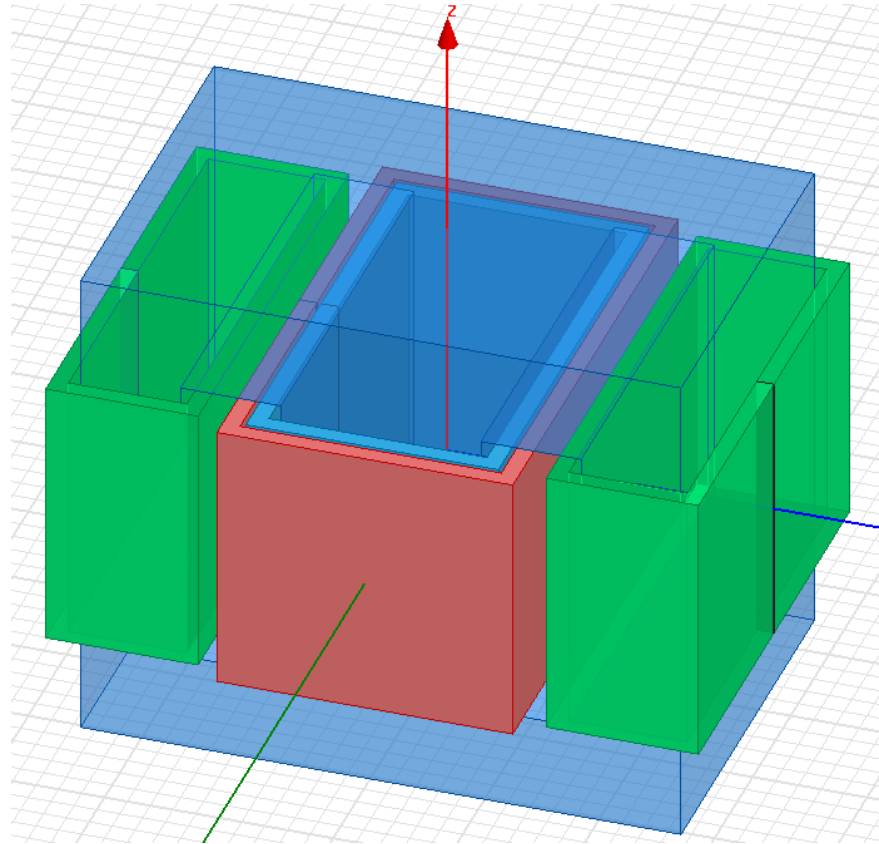
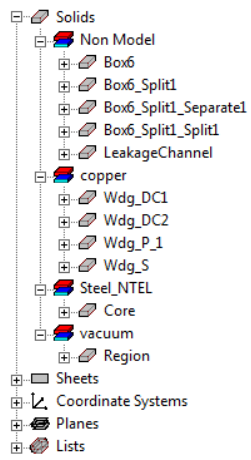
| H (A/m)  | B (T)    | H (A/m)  | B (T) | H (A/m)  | B (T) | H (A/m)  | B (T) | H (A/m)  | B (T) | H (A/m)  | B (T) |
|----------|----------|----------|-------|----------|-------|----------|-------|----------|-------|----------|-------|
| 0.000    | 0.00     | 41.11163 | 0.34  | 67.24481 | 0.70  | 118.5864 | 1.06  | 511.7721 | 1.42  | 8779.73  | 1.78  |
| 0.010    | 1.15E-05 | 41.73618 | 0.35  | 68.17687 | 0.71  | 120.9238 | 1.07  | 558.5958 | 1.43  | 9283.186 | 1.79  |
| 0.100    | 0.000128 | 42.36091 | 0.36  | 69.12617 | 0.72  | 123.3544 | 1.08  | 611.5716 | 1.44  | 9795.503 | 1.80  |
| 0.500    | 0.000721 | 42.98645 | 0.37  | 70.09331 | 0.73  | 125.8857 | 1.09  | 671.4106 | 1.45  | 10328.46 | 1.81  |
| 1.000    | 0.001591 | 43.61342 | 0.38  | 71.07892 | 0.74  | 128.5259 | 1.10  | 738.8469 | 1.46  | 10912.16 | 1.82  |
| 2.000    | 0.003682 | 44.24241 | 0.39  | 72.08365 | 0.75  | 131.2843 | 1.11  | 814.6181 | 1.47  | 11535.13 | 1.83  |
| 3.000    | 0.006101 | 44.87395 | 0.40  | 73.10818 | 0.76  | 134.1713 | 1.12  | 899.4411 | 1.48  | 12180.44 | 1.84  |
| 4.000    | 0.008721 | 45.50858 | 0.41  | 74.15321 | 0.77  | 137.1985 | 1.13  | 993.9834 | 1.49  | 12851.88 | 1.85  |
| 5.000    | 0.011598 | 46.14679 | 0.42  | 75.21949 | 0.78  | 140.3793 | 1.14  | 1098.833 | 1.50  | 13554.2  | 1.86  |
| 6.000    | 0.014821 | 46.78909 | 0.43  | 76.30779 | 0.79  | 143.7286 | 1.15  | 1214.467 | 1.51  | 14303.39 | 1.87  |
| 7.000    | 0.018261 | 47.43592 | 0.44  | 77.4189  | 0.80  | 147.2634 | 1.16  | 1341.226 | 1.52  | 15107.11 | 1.88  |
| 8.000    | 0.021901 | 48.08776 | 0.45  | 78.5537  | 0.81  | 151.0031 | 1.17  | 1479.298 | 1.53  | 15975.23 | 1.89  |
| 9.000    | 0.025821 | 48.74504 | 0.46  | 79.71305 | 0.82  | 154.9698 | 1.18  | 1628.711 | 1.54  | 16920.62 | 1.90  |
| 10.000   | 0.029861 | 49.4082  | 0.47  | 80.89791 | 0.83  | 159.1885 | 1.19  | 1789.344 | 1.55  | 17960.09 | 1.91  |
| 15.000   | 0.05421  | 50.07766 | 0.48  | 82.10925 | 0.84  | 163.6882 | 1.20  | 1960.954 | 1.56  | 19115.77 | 1.92  |
| 21.986   | 0.0955   | 50.75384 | 0.49  | 83.34813 | 0.85  | 168.5018 | 1.21  | 2143.218 | 1.57  | 20416.9  | 1.93  |
| 24.212   | 0.1125   | 51.43716 | 0.50  | 84.61565 | 0.86  | 173.6672 | 1.22  | 2335.785 | 1.58  | 21902.14 | 1.94  |
| 25.851   | 0.1271   | 52.12803 | 0.51  | 85.91297 | 0.87  | 179.228  | 1.23  | 2538.336 | 1.59  | 23622.53 | 1.95  |
| 27.73    | 0.14609  | 52.82685 | 0.52  | 87.24134 | 0.88  | 185.2344 | 1.24  | 2750.639 | 1.60  | 25645.23 | 1.96  |
| 28.951   | 0.16118  | 53.53403 | 0.53  | 88.60209 | 0.89  | 191.7442 | 1.25  | 2972.601 | 1.61  | 28057.78 | 1.97  |
| 30.616   | 0.18273  | 54.24998 | 0.54  | 89.99661 | 0.90  | 198.8243 | 1.26  | 3204.294 | 1.62  | 30972.64 | 1.98  |
| 31.2375  | 0.19099  | 54.9751  | 0.55  | 91.42642 | 0.91  | 206.5518 | 1.27  | 3445.979 | 1.63  | 34530.82 | 1.99  |
| 31.87142 | 0.19963  | 55.70981 | 0.56  | 92.89313 | 0.92  | 215.0162 | 1.28  | 3698.09  | 1.64  | 39000    | 2.00  |
| 32.60154 | 0.2099   | 56.45452 | 0.57  | 94.39846 | 0.93  | 224.3205 | 1.29  | 3961.209 | 1.65  | 63600    | 2.05  |
| 33.31374 | 0.22     | 57.20963 | 0.58  | 95.94426 | 0.94  | 234.5844 | 1.30  | 4236.009 | 1.66  | 90000    | 2.10  |
| 34.01037 | 0.23     | 57.97559 | 0.59  | 97.53256 | 0.95  | 245.9462 | 1.31  | 4523.175 | 1.67  | 146900   | 2.20  |
| 34.69351 | 0.24     | 58.7528  | 0.60  | 99.16549 | 0.96  | 258.5657 | 1.32  | 4823.296 | 1.68  | 205000   | 2.30  |
| 35.36503 | 0.25     | 59.54172 | 0.61  | 100.8454 | 0.97  | 272.6278 | 1.33  | 5136.727 | 1.69  | 330000   | 2.50  |
| 36.02657 | 0.26     | 60.34277 | 0.62  | 102.5749 | 0.98  | 288.3454 | 1.34  | 5463.418 | 1.70  | 550000   | 2.80  |
| 36.67962 | 0.27     | 61.15642 | 0.63  | 104.3566 | 0.99  | 305.964  | 1.35  | 5806.325 | 1.71  | 706650   | 3.00  |
| 37.32551 | 0.28     | 61.98312 | 0.64  | 106.1936 | 1.00  | 325.7651 | 1.36  | 6169.648 | 1.72  | 2300000  | 5.01  |
| 37.96546 | 0.29     | 62.82334 | 0.65  | 108.0893 | 1.01  | 348.071  | 1.37  | 6558.21  | 1.73  | 5475000  | 9.00  |
| 38.60057 | 0.30     | 63.67758 | 0.66  | 110.0471 | 1.02  | 373.2485 | 1.38  | 6962.792 | 1.74  |          |       |
| 39.23185 | 0.31     | 64.54632 | 0.67  | 112.0712 | 1.03  | 401.7131 | 1.39  | 7385.245 | 1.75  |          |       |
| 39.86023 | 0.32     | 65.43009 | 0.68  | 114.1657 | 1.04  | 433.9322 | 1.40  | 7828.505 | 1.76  |          |       |
| 40.48656 | 0.33     | 66.3294  | 0.69  | 116.3357 | 1.05  | 470.4267 | 1.41  | 8291.611 | 1.77  |          |       |

**Table A-3. B-H curve data of the core material of Prototype 2.**

| <b>H (A/m)</b> | <b>B (T)</b> | <b>H (A/m)</b> | <b>B (T)</b> | <b>H (A/m)</b> | <b>B (T)</b> | <b>H (A/m)</b> | <b>B (T)</b> |
|----------------|--------------|----------------|--------------|----------------|--------------|----------------|--------------|
| 0.000          | 0.00         | 6.637876       | 0.36         | 20.83269       | 0.72         | 185.811        | 1.08         |
| 0.181369       | 0.01         | 6.834387       | 0.37         | 21.89599       | 0.73         | 197.0182       | 1.09         |
| 0.362758       | 0.02         | 7.032863       | 0.38         | 23.05136       | 0.74         | 209.1377       | 1.10         |
| 0.54417        | 0.03         | 7.233548       | 0.39         | 24.30698       | 0.75         | 222.3674       | 1.11         |
| 0.725608       | 0.04         | 7.436716       | 0.40         | 25.67149       | 0.76         | 236.9647       | 1.12         |
| 0.907076       | 0.05         | 7.642672       | 0.41         | 27.15399       | 0.77         | 253.2618       | 1.13         |
| 1.088579       | 0.06         | 7.851759       | 0.42         | 28.76396       | 0.78         | 271.6848       | 1.14         |
| 1.270122       | 0.07         | 8.064361       | 0.43         | 30.5113        | 0.79         | 292.7765       | 1.15         |
| 1.451711       | 0.08         | 8.280907       | 0.44         | 32.4062        | 0.80         | 317.2221       | 1.16         |
| 1.633353       | 0.09         | 8.501877       | 0.45         | 34.4591        | 0.81         | 345.8768       | 1.17         |
| 1.815055       | 0.10         | 8.727805       | 0.46         | 36.68064       | 0.82         | 379.7963       | 1.18         |
| 1.996826       | 0.11         | 8.959292       | 0.47         | 39.08157       | 0.83         | 420.2682       | 1.19         |
| 2.178677       | 0.12         | 9.197004       | 0.48         | 41.67263       | 0.84         | 468.8487       | 1.20         |
| 2.360617       | 0.13         | 9.441687       | 0.49         | 44.46448       | 0.85         | 587            | 1.22         |
| 2.54266        | 0.14         | 9.694174       | 0.50         | 47.46763       | 0.86         | 736            | 1.24         |
| 2.72482        | 0.15         | 9.955388       | 0.51         | 50.69226       | 0.87         | 933            | 1.26         |
| 2.907114       | 0.16         | 10.22636       | 0.52         | 54.14823       | 0.88         | 1215           | 1.28         |
| 3.089558       | 0.17         | 10.50825       | 0.53         | 57.84494       | 0.89         | 1702           | 1.30         |
| 3.272175       | 0.18         | 10.80232       | 0.54         | 61.79126       | 0.90         | 7000           | 1.40         |
| 3.454988       | 0.19         | 11.10999       | 0.55         | 65.99555       | 0.91         | 15000          | 1.50         |
| 3.638022       | 0.20         | 11.43284       | 0.56         | 70.46558       | 0.92         | 28000          | 1.60         |
| 3.821307       | 0.21         | 11.77261       | 0.57         | 75.20864       | 0.93         | 51000          | 1.70         |
| 4.004878       | 0.22         | 12.13123       | 0.58         | 80.23152       | 0.94         | 88000          | 1.80         |
| 4.188771       | 0.23         | 12.51086       | 0.59         | 85.54072       | 0.95         | 150000         | 1.90         |
| 4.373029       | 0.24         | 12.91384       | 0.60         | 91.14263       | 0.96         | 220000         | 2.00         |
| 4.557701       | 0.25         | 13.34279       | 0.61         | 97.0438        | 0.97         | 950000         | 3.00         |
| 4.742839       | 0.26         | 13.80059       | 0.62         | 103.2513       | 0.98         | 2540500        | 5.00         |
| 4.928506       | 0.27         | 14.29039       | 0.63         | 109.7734       | 0.99         |                |              |
| 5.114768       | 0.28         | 14.81568       | 0.64         | 116.6198       | 1.00         |                |              |
| 5.301704       | 0.29         | 15.38025       | 0.65         | 123.8032       | 1.01         |                |              |
| 5.489399       | 0.30         | 15.98828       | 0.66         | 131.3396       | 1.02         |                |              |
| 5.67795        | 0.31         | 16.6443        | 0.67         | 139.2505       | 1.03         |                |              |
| 5.867467       | 0.32         | 17.35326       | 0.68         | 147.5641       | 1.04         |                |              |
| 6.058072       | 0.33         | 18.12054       | 0.69         | 156.3182       | 1.05         |                |              |
| 6.249903       | 0.34         | 18.95195       | 0.70         | 165.5628       | 1.06         |                |              |
| 6.443113       | 0.35         | 19.85375       | 0.71         | 175.3645       | 1.07         |                |              |

## APPENDIX B. FEA MODEL SETUP

List of component objects



Primary winding setup

| Name                | Value  | Unit | Evaluated Value |
|---------------------|--|------|-----------------|
| Name                | primary  |      |                 |
| Type                | Winding Group  |      |                 |
| Winding Type        | Voltage  |      |                 |
| IsSolid             | Stranded   |      |                 |
| Initial Current     | 0  | A    | 0A              |
| Resistance          | 0.15   | ohm  | 0.15ohm         |
| Inductance          | 0  | mH   | 0mH             |
| Voltage             | $20.9 \cdot \sqrt{2} \cdot \cos(120 \cdot \pi \cdot \text{Time}) \cdot f(\text{Time} < 0.05, 20 \cdot \text{Time}, 1)$ |      | *****           |
| Number of Parall... | 1  |      | 1               |

### Primary winding coil terminal

| Name              | Value                 | Unit | Evaluated Value |
|-------------------|-----------------------|------|-----------------|
| Name              | pmy                   |      |                 |
| Type              | Coil Terminal         |      |                 |
| Number of Cond... | NpmTums               |      | 95              |
| Direction         | Point out of terminal |      |                 |

### Secondary winding setup

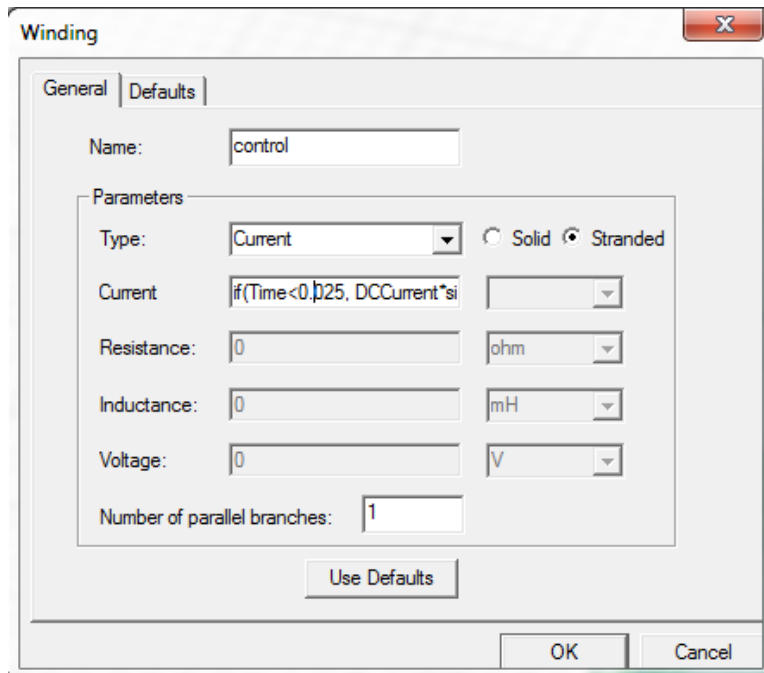
| Name              | Value                 | Unit | Evaluated Value |
|-------------------|-----------------------|------|-----------------|
| Name              | scnd                  |      |                 |
| Type              | Coil Terminal         |      |                 |
| Number of Cond... | NscdTums              |      | 98              |
| Direction         | Point out of terminal |      |                 |

### Secondary winding coil terminal

| Name                | Value         | Unit | Evaluated Value |
|---------------------|---------------|------|-----------------|
| Name                | secondary     |      |                 |
| Type                | Winding Group |      |                 |
| Winding Type        | Voltage       |      |                 |
| IsSolid             | Stranded      |      |                 |
| Initial Current     | 0             | A    | 0A              |
| Resistance          | 56            | ohm  | 56ohm           |
| Inductance          | 0             | mH   | 0mH             |
| Voltage             | 0             | V    | 0V              |
| Number of Parall... | 1             |      | 1               |



## DC winding setup



The 'Winding' dialog box is shown with the 'General' tab selected. It contains a 'Name' field with the value 'control'. Below this is a 'Parameters' section with several fields: 'Type' is a dropdown menu set to 'Current'; 'Current' is a text field containing the expression 'if(Time<0.025, DCCurrent\*si'; 'Resistance' is a text field with '0' and a unit dropdown set to 'ohm'; 'Inductance' is a text field with '0' and a unit dropdown set to 'mH'; 'Voltage' is a text field with '0' and a unit dropdown set to 'V'; and 'Number of parallel branches' is a text field with '1'. There are radio buttons for 'Solid' and 'Stranded', with 'Stranded' being selected. A 'Use Defaults' button is located below the parameters section. At the bottom of the dialog are 'OK' and 'Cancel' buttons.

Winding

General Defaults

Name: control

Parameters

Type: Current ☐ Solid ☒ Stranded

Current: if(Time<0.025, DCCurrent\*si

Resistance: 0 ohm

Inductance: 0 mH

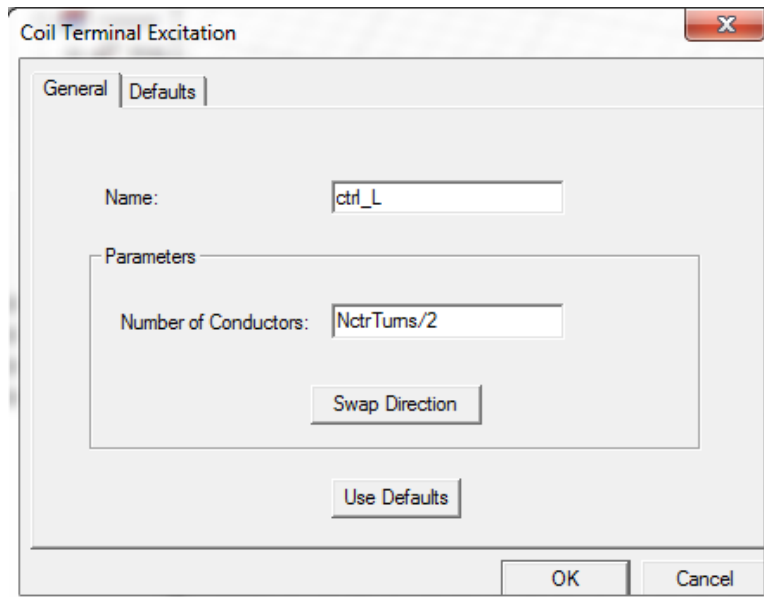
Voltage: 0 V

Number of parallel branches: 1

Use Defaults

OK Cancel

## DC coil support coil terminal setup



The 'Coil Terminal Excitation' dialog box is shown with the 'General' tab selected. It contains a 'Name' field with the value 'ctrl\_L'. Below this is a 'Parameters' section with a 'Number of Conductors' text field containing the expression 'NctrTums/2'. There is a 'Swap Direction' button. A 'Use Defaults' button is located below the parameters section. At the bottom of the dialog are 'OK' and 'Cancel' buttons.

Coil Terminal Excitation

General Defaults

Name: ctrl\_L

Parameters

Number of Conductors: NctrTums/2

Swap Direction

Use Defaults

OK Cancel

## APPENDIX C. NETL TESTING REPORT

Manufacturer: Triad Magnetics

Part Number: N-57MG

Description: Power Transformers Power Transformer, Isolation, 115 VAC (Nominal Secondary) Output, 115 VAC Input, 500 W (V A Rating) Output, Electrical Specifications (@25°C)

1. Maximum Power: 500 VA
2. Input Voltage: 115 V, 50/60 Hz
3. Output Voltage: 115 V + 5%
4. Full Secondary Load: 4.35 Amps RMS
5. Voltage Regulation: 5 % TYP @ full load to no load

<https://catalog.triadmagnetics.com/item/power-transformers/isolation-power-transformers/n-57mg-1>

### Measured specification by NETL:

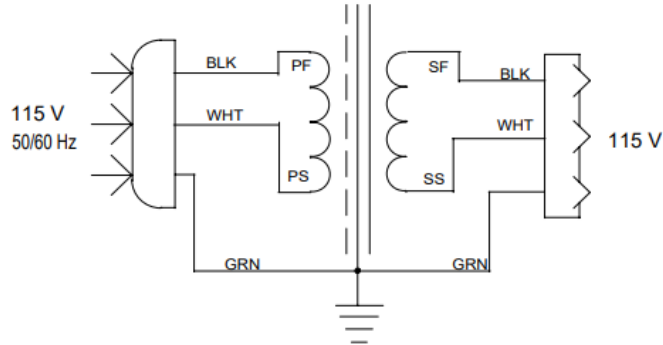
#### Lamination thickness:

3.5 in./27 layers = about 0.13 in./layer (88.9 mm/27 layers = about 3.3 mm/layer)

**EI-175 core dimensions:** This is not the identical part as the transformer under test. Please use this information only for the dimension information.

[http://www.tempel.com/images/uploads/documents\\_pdfs/TempelTransformerCatalogue.pdf](http://www.tempel.com/images/uploads/documents_pdfs/TempelTransformerCatalogue.pdf)

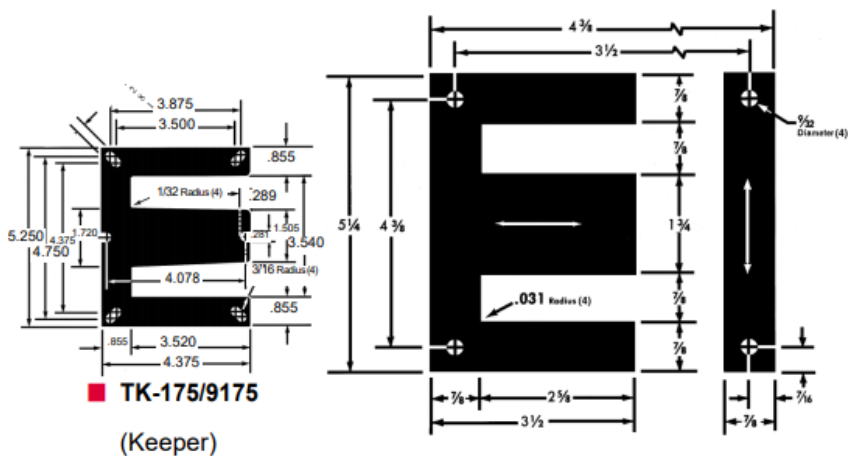
page 23, EI-175 cores



| SPECIFICATIONS APPLYING TO CORE STACK WITH SQUARE CROSS SECTIONS |                      |                  |                 |
|--|----------------------|------------------|-----------------|
| Window Dimensions  | 2.625 in. x .875 in. | 2.297 sq. in. –  | 14.819 sq. cm.  |
| Volume, solid  |                      | 31.721 cu. in. – | 519.821 cu. cm. |
| Cross Sectional Area, solid                                      |                      | 3.063 sq. in. –  | 19.758 sq. cm.  |
| Length of Magnetic Path  |                      | 10.500 in. –     | 26.670 cm.      |

#### METRIC EQUIVALENTS

| Inches | Millimeters |
|--------|-------------|
| .031   | 0.7874      |
| 9/32   | 7.1438      |
| 7/16   | 11.1125     |
| 7/8    | 22.2250     |
| 1-3/4  | 44.4500     |
| 2-5/8  | 66.6750     |
| 3-1/2  | 88.9000     |
| 4-3/8  | 111.1250    |
| 5-1/4  | 133.3500    |



| SPECIFICATIONS APPLYING TO CORE STACK WITH SQUARE CROSS SECTIONS |                      |                  |                 |
|--|----------------------|------------------|-----------------|
| Window Dimensions  | 2.625 in. x .875 in. | 2.297 sq. in. –  | 14.819 sq. cm.  |
| Volume, solid  |                      | 31.721 cu. in. – | 519.821 cu. cm. |
| Cross Sectional Area, solid                                      |                      | 3.063 sq. in. –  | 19.758 sq. cm.  |
| Length of Magnetic Path  |                      | 10.500 in. –     | 26.670 cm.      |

Mean path = 0.2667 m

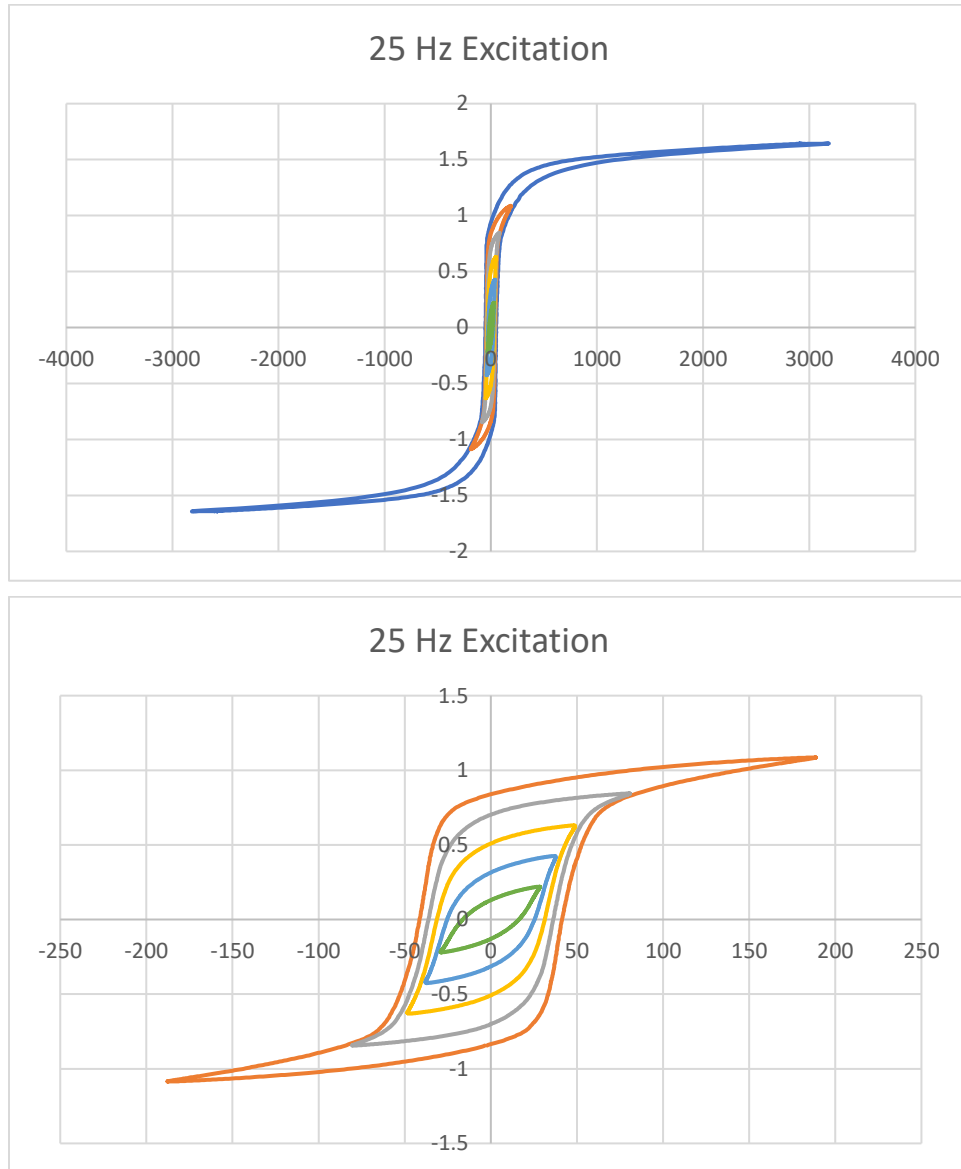
Cross-section = 0.0039516 m<sup>2</sup>

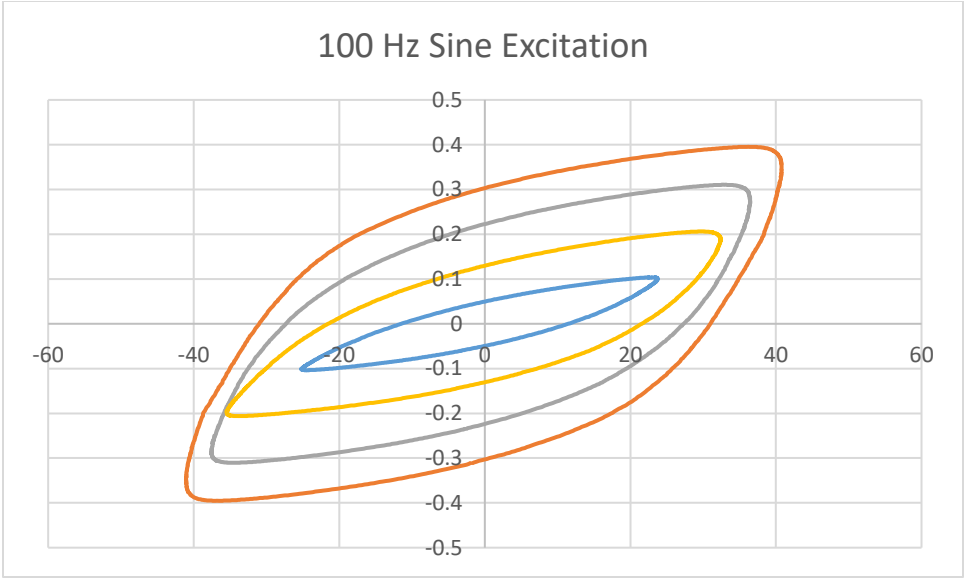
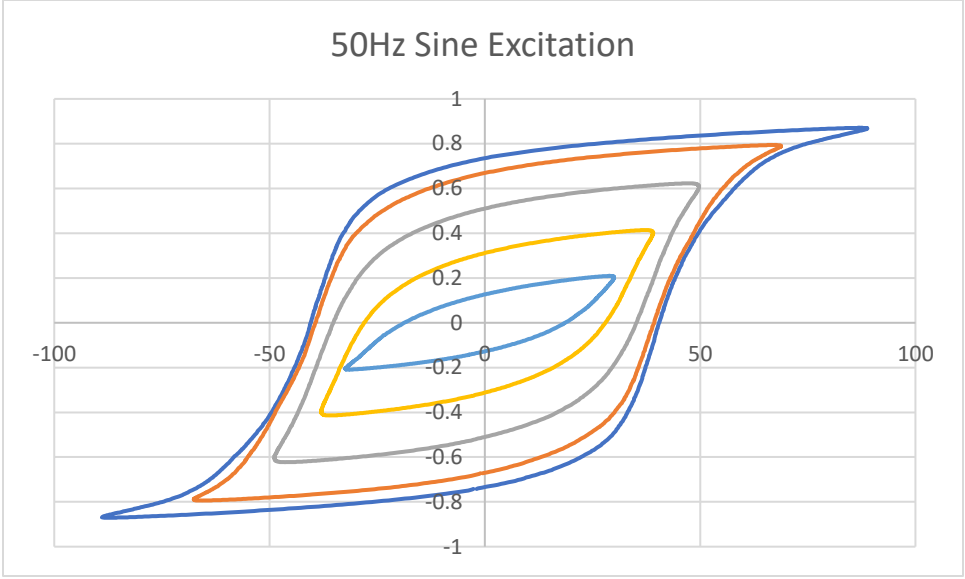
Measured number of turns: Primary = 94.25; Secondary = 98.2

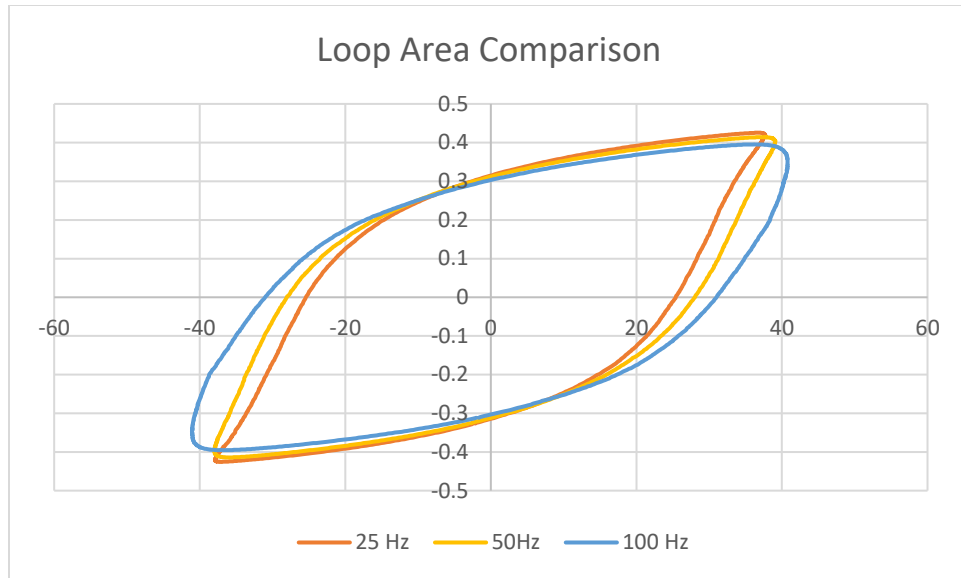
EI-175H / 0175

23

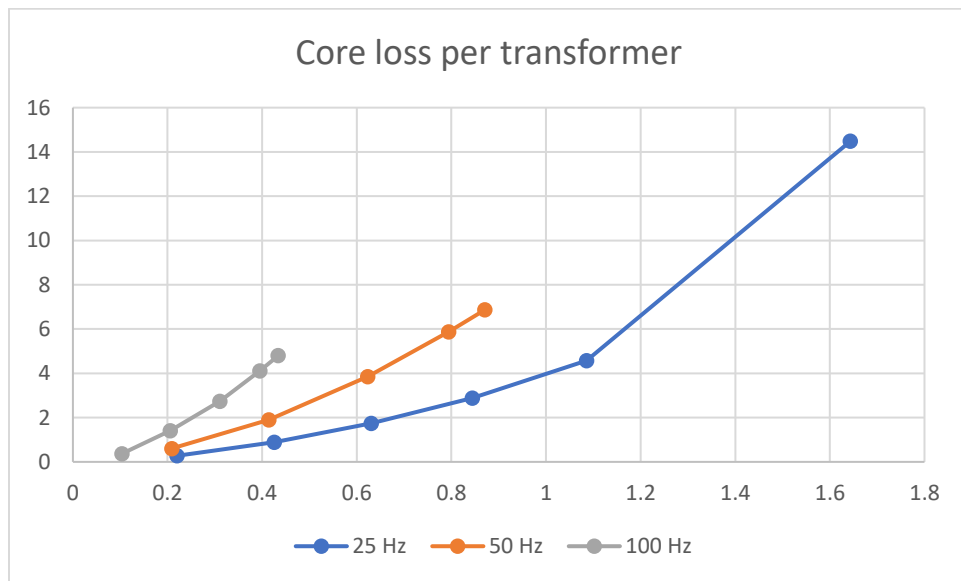
## B-H loops

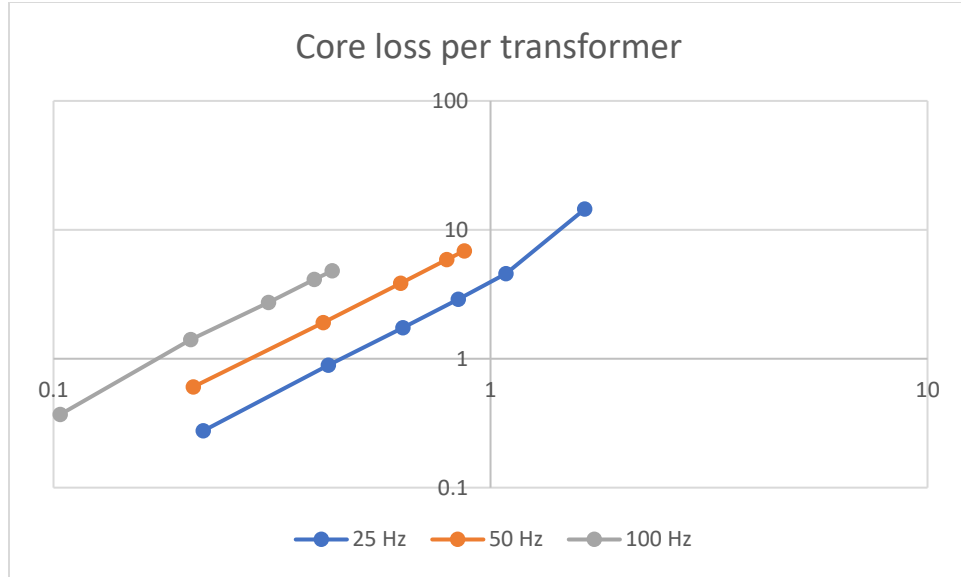






## Core losses



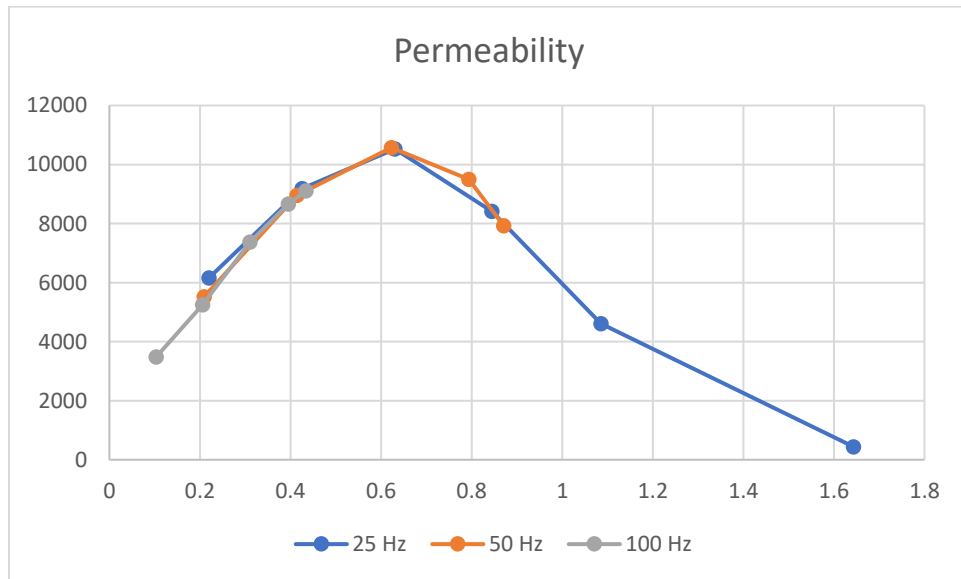


### Permeability

The permeability of the core is measured as a function of flux density and frequency. The measured absolute relative permeability  $\mu_r$  values is defined as

$$\mu_r = \frac{B_{peak}}{\mu_0 H_{peak}} \quad (A2.1)$$

where  $B_{peak}$  and  $H_{peak}$  are the maximum flux density and field strength at each measurement point.



### Anhyysteritic B-H curves

Figure A2.1 illustrates the measured low frequency B-H loops at 25 Hz. Using the outer most B-H loop, the anhyysteretic B-H curve is fitted. The anhyysteretic B-H curves can be computed as a function of field intensity H using the follow formula.

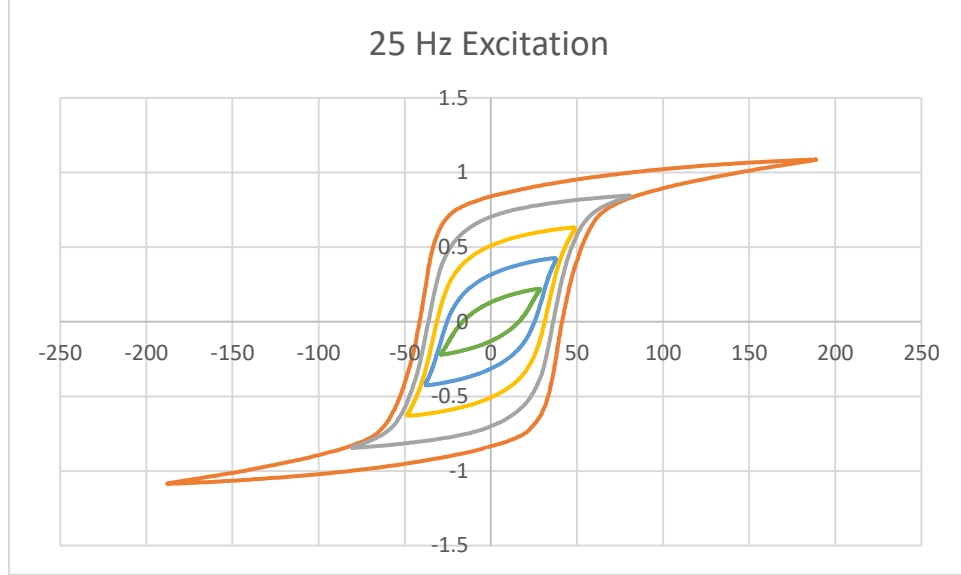


**Figure A2.1. Low frequency B-H loops (excitation at 25 Hz).**

$$B = \mu_H(H)H$$

$$\mu_H(H) = \mu_0 + \sum_{k=1}^K \frac{m_k}{h_k} \frac{1}{1 + |H/h_k|^{n_k}} \quad (\text{A2.2})$$

Similarly, the anhyysteretic B-H curves can be computed as a function of flux density B using the following formula.

$$B = \mu_B(B)H$$

$$\mu_B(B) = \mu_0 \frac{r(B)}{r(B) - 1}$$

$$r(B) = \frac{\mu_r}{\mu_r - 1} + \sum_{k=1}^K \alpha_k |B| + \delta_k \ln(\varepsilon_k + \zeta_k e^{-\beta_k |B|}) \quad (\text{A2.3})$$

$$\delta_k = \frac{\alpha_k}{\beta_k}, \varepsilon_k = \frac{e^{-\beta_k \gamma_k}}{1 + e^{-\beta_k \gamma_k}}, \zeta_k = \frac{1}{1 + e^{-\beta_k \gamma_k}}$$

Table A2.2 and Table A2.3 list the anhyysteretic curve coefficients for Eqs. (A2.2) and (A2.3), respectively. The core anhyysteretic characteristic models in (A2.2) and (A2.3) are based on the following references.

S. D. Sudhoff, "Magnetics and Magnetic Equivalent Circuits," *Power Magnetic Devices: A Multi-Objective Design Approach*, Hoboken, New Jersey, USA: Wiley-IEEE Press, pp. 488–490, 2014.



G. M. Shane and S. D. Sudhoff, “Refinements in Anhysteretic Characterization and Permeability Modeling,” *IEEE Transactions on Magnetics*, vol. 46, no. 11, pp. 3834–3843, Nov. 2010.

The estimation of the anhysteretic characteristic is performed using a genetic optimization program, which can be found in the following website:

[https://engineering.purdue.edu/ECE/Research/Areas/PEDS/go\\_system\\_engineering\\_toolbox](https://engineering.purdue.edu/ECE/Research/Areas/PEDS/go_system_engineering_toolbox)

**Table A2.2. Anhysteretic curve coefficients for B as a function of H.**

| $k$   | 1                | 2                 | 3                   | 4                 |
|-------|------------------|-------------------|---------------------|-------------------|
| $m_k$ | 1.35678557834430 | 0.166860185860400 | −0.0689489475247155 | 0.516790783208244 |
| $h_k$ | 45.5032785300985 | 12.7545530775786  | 48.7041963447760    | 22.9942869378183  |
| $n_k$ | 1                | 2.59839836613898  | 1.10000076593992    | 2.22875760493294  |

**Table A2.3. Anhysteretic curve coefficients for H as a function of B.**

| $k$             | 1                     | 2                    | 3                    | 4                    |
|-----------------|-----------------------|----------------------|----------------------|----------------------|
| $\mu_r$         | 4.387804250163725e+04 |                      |                      |                      |
| $\alpha_k$      | 0.688548931226430     | 0.0336477128975609   | 0.0243820757741031   | 0.00100000074228011  |
| $\beta_k$       | 78.3257436605065      | 104.787161555768     | 26.2629467608963     | 10.0431118022472     |
| $\gamma_k$      | 1.31958902563931      | 1.51782267220448     | 1.26016865022958     | 0.911503516522646    |
| $\delta_k$      | 0.00879083809546530   | 0.000321105299523295 | 0.000928383094101470 | 9.95708065359141e-05 |
| $\varepsilon_k$ | 0.00879083809546530   | 0.000321105299523295 | 0.000928383094101470 | 9.95708065359141e-05 |
| $\zeta_k$       | 1                     | 1                    | 0.999999999999996    | 0.999894250501215    |

Figure A2.6.1 illustrates the measured B-H curve and fitted anhysteretic B-H curves as functions of H and B using the coefficients from Table A2.2 and Table A2.3. Figure A2.6.2 and Figure A2.6.3 illustrate the absolute relative permeability as functions of field strength H and flux density B, respectively. Figure A2.6.4 illustrates the incremental relative permeability.

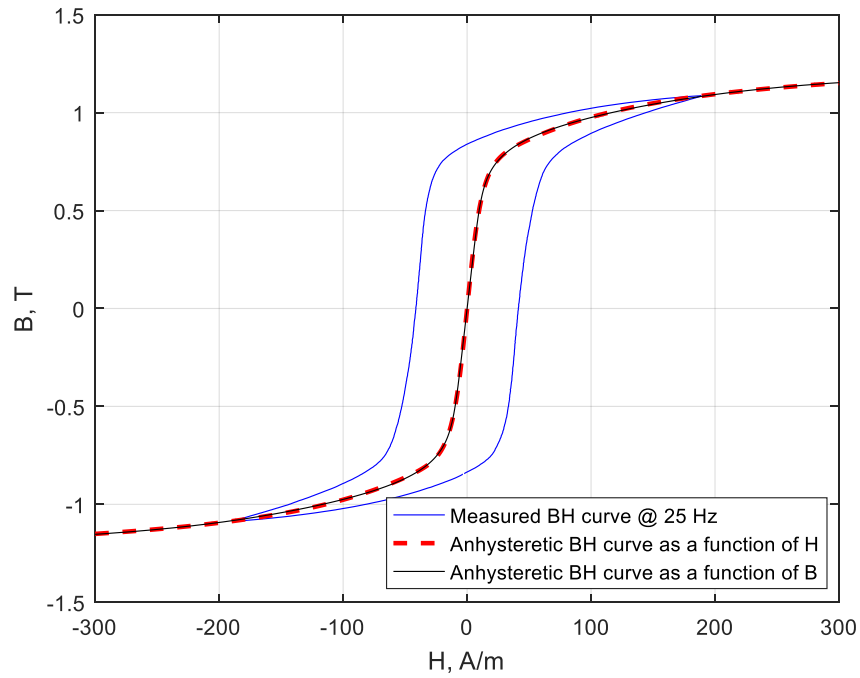


**Figure A2.6.1. Measured B-H curve and fitted anhysteretic B-H curve as functions of H and B.**

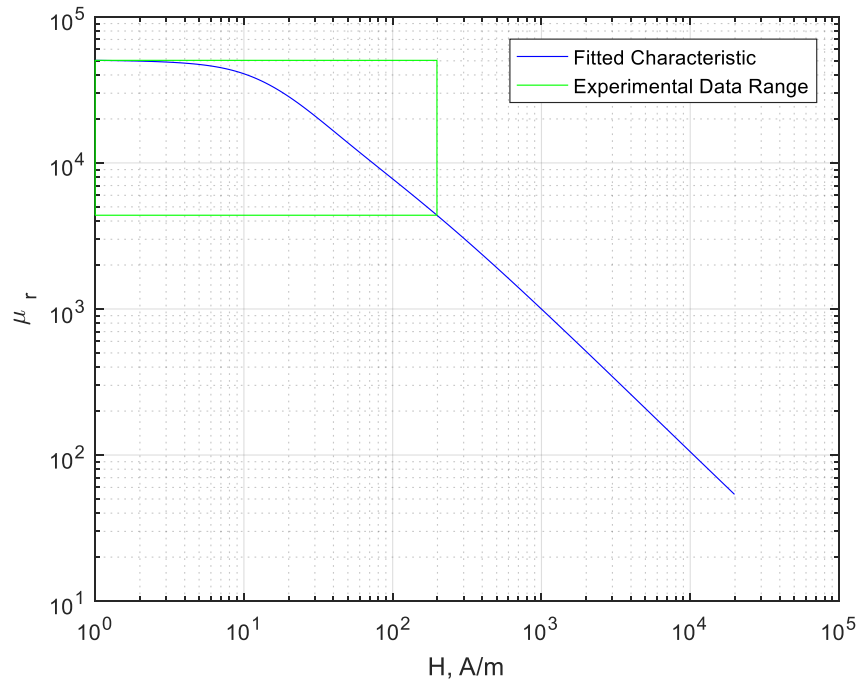


**Figure A2.6.2. Absolute relative permeability as a function of field strength H.**

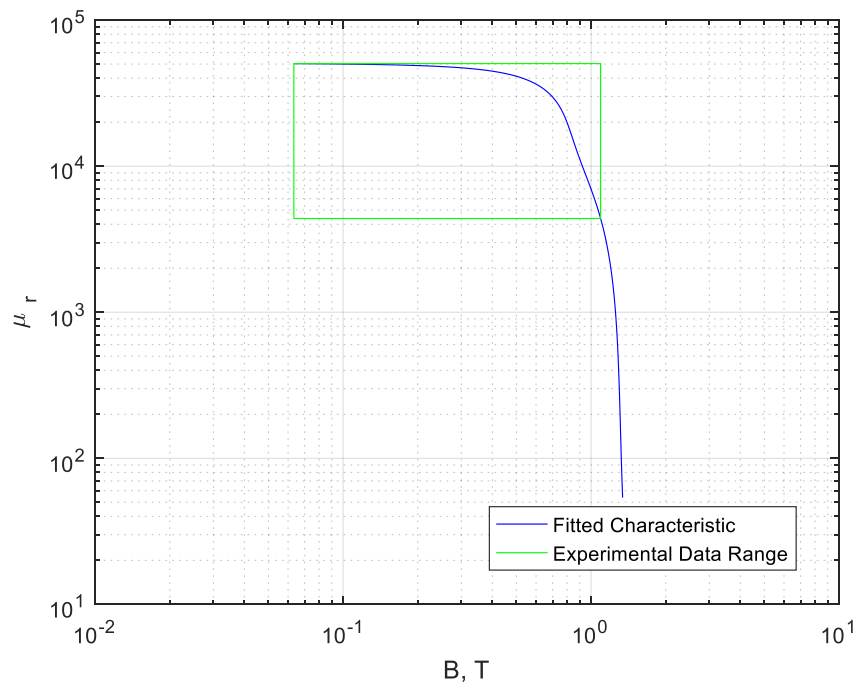


**Figure A2.6.3 Absolute relative permeability as a function of flux density  $B$ .**

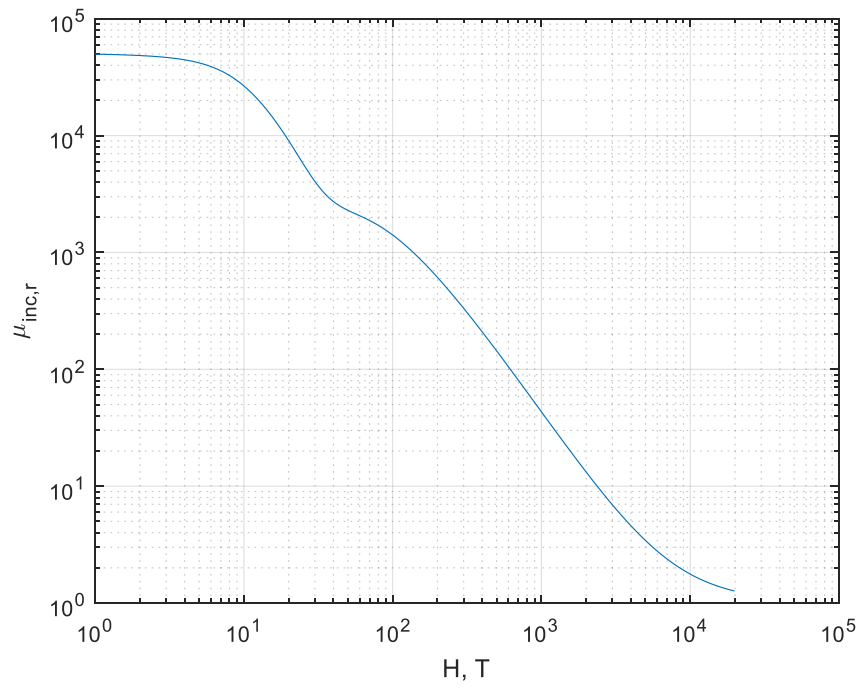
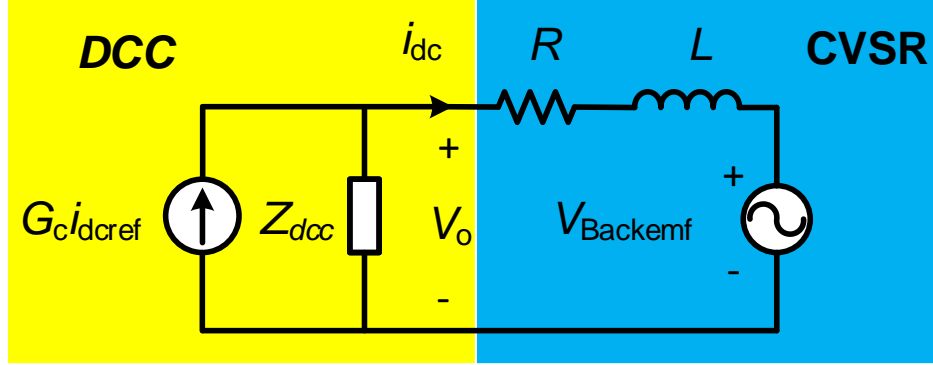


**Figure A2.6.4. Incremental relative permeability.**

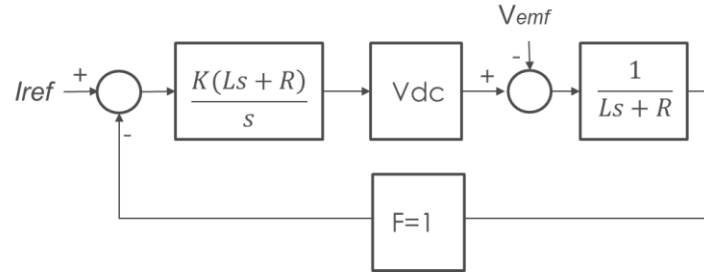
## APPENDIX D. DERIVATION OF THE TIME-DOMAIN MODEL OF A DC SOURCE

### Approach 1

The equivalent circuit of the DC controller discussed in Section 4.2 for integration into the TAREX model is shown below.



The diagram of its s-domain control loop is



The increment of DC output current  $i_{dc}$  can be obtained by

$$i_{dc}(s) = G_1(s) \cdot I_{ref} + G_2(s) \cdot V_{emf}(s) \quad (A4.1)$$

where  $G_1(s)$  and  $G_2(s)$  are the system gains when  $V_{emf} = 0$  and  $I_{ref} = 0$  are assumed, respectively. Based on the control diagram, the two gains can be obtained as

$$G_1(s) \Big|_{V_{emf}=0} = \frac{KV_{dc}}{s+P_1} \text{ and } G_2(s) \Big|_{I_{ref}=0} = -\frac{s/L}{(s+P_1)(s+P_2)} \quad (A4.2)$$

where  $P_1$  and  $P_2$  are the two poles of the system:  $P_1 = KV_{dc}F$ ,  $P_2 = R/L$ .  $P_1$  is related to the DC control and  $P_2$  to the external (dc winding) circuit. Inserting Eq. (A4.2) into Eq. (A4.1),  $i_{dc}$  can be rewritten as

$$i_{dc}(s) = \frac{a_1}{s+P_1} + \frac{a_2}{s+P_2} \quad (A4.3)$$

where

$$a_1 = KV_{dc} \left( I_{ref} + \frac{FV_{emf}(s)}{R - KV_{dc}FL} \right)$$

$$a_2 = -\frac{RV_{emf}(s)}{(R - KV_{dc}FL)L}$$

Equation (A4.3) is not the final form of the formula because the induced voltage term ( $V_{emf}$ ) is still  $s$ -dependent.  $V_{emf}$  can be calculated by subtracting the two voltages induced on the two DC coils. It is difficult to obtain the exact analytical expression of  $V_{emf}$  because the two DC coil induced voltages are nonlinear when the DC bias is present. However, the authors knew from previous studies that the 2<sup>nd</sup> harmonics dominates in  $V_{emf}$ , and thus  $V_{emf}$  can be simplified as

$$V_{emf}(s) = \frac{sV_{e0}}{s^2 + \omega^2} \quad (A4.4)$$

which is the Laplace transform of a cosine wave with the frequency of 120Hz and amplitude of  $V_{e0}$ . With Eq. (A4.4) inserted and some algebra manipulations, Eq. (A.3) can be rewritten as

$$i_{dc}(s) = \frac{KV_{dc}I_{ref}}{s + P_1} + \frac{KV_{dc}FV_{e0}}{R - KV_{dc}FL} \cdot \frac{s}{(s + P_1)(s^2 + \omega^2)} - \frac{RV_{e0}/L}{R - KV_{dc}FL} \cdot \frac{s}{(s + P_2)(s^2 + \omega^2)} \quad (A4.5)$$

Applying the inverse Laplace transform to Eq. (A4.5), the time-domain equation of the increment  $i_{dc}$  can be obtained as

$$i_{dc}(t) = b_1 e^{-P_1 t} + b_2 e^{-P_2 t} + c_1 \cos(\omega t) + c_2 \sin(\omega t) \quad (A4.6)$$

where

$$b_1 = KV_{dc} \left[ I_{ref} - \frac{FV_{e0}P_1}{(R - KV_{dc}FL)(P_1^2 + \omega^2)} \right]$$

$$b_2 = \frac{RV_{e0}P_2/L}{(R - KV_{dc}FL)(P_2^2 + \omega^2)}$$

$$c_1 = \frac{V_{e0}}{R - KV_{dc}FL} \left( \frac{KV_{dc}FP_1}{P_1^2 + \omega^2} - \frac{RP_2/L}{P_2^2 + \omega^2} \right)$$

$$c_2 = \frac{\omega V_{e0}}{R - KV_{dc}FL} \left( \frac{KV_{dc}F}{P_1^2 + \omega^2} - \frac{R/L}{P_2^2 + \omega^2} \right)$$

Equation (A4.6) is to determine the ripples imposed on the setting value of the DC control ( $I_{ref}$ ). The first two exponential terms decay to zero eventually. At a steady state, the increment  $i_{dc}$  is the sum of a cosine and a sine term. To integrate the DC control into the TAREX model, Eq. (A4.6) will be solved together with the time-domain analytical equations of the TAREX.

## Approach 2

Assuming the output voltage  $V_o$  of the DC controller (DCC) is constant (at least for the dc component of  $i_{dc}$ ), the dynamics in the DC winding circuit can be obtained by solving the differential equation of

$$Ri_{dc}(t) + L \frac{d[i_{dc}(t)]}{dt} + V_{emf} = 0 \quad (\text{A4.7})$$

where  $i_{dc}(t)$  is the AC component of the DC winding current.

Solving Eq. (A4.7) with the other electric/magnetic circuit equations will give the dynamics in the TAREX. However, by assuming constant  $V_o$ , this approach does not provide any insight of the details of the interaction between the DC controller and the TAREX device.